An International Standard Formulation for the Thermodynamic Properties of 1,1,1-Trifluoroethane (HFC-143a) for Temperatures From 161 to 450 K and Pressures to 50 MPa

Cite as: Journal of Physical and Chemical Reference Data **29**, 521 (2000); https://doi.org/10.1063/1.1318909
Submitted: 09 November 1999 . Accepted: 26 July 2000 . Published Online: 05 March 2001

Eric W. Lemmon, and Richard T Jacobsen

An International Standard Formulation for the Thermodynamic Properties of 1,1,1-Trifluoroethane (HFC-143a) for Temperatures From 161 to 450 K and Pressures to 50 MPa

Eric W. Lemmon[a)]

Physical and Chemical Properties Division, National Institute of Standards and Technology, 325 Broadway, Boulder, Colorado 80305

Richard T Jacobsen

Center for Applied Thermodynamic Studies, College of Engineering, University of Idaho, Moscow, Idaho 83844

Received November 9, 1999; accepted July 26, 2000

A new formulation is presented for the thermodynamic properties of refrigerant 143a (1,1,1-trifluoroethane, CH_3–CF_3) based upon available experimental data. The formulation can be used for the calculation of density, heat capacity, speed of sound, energy, and saturation properties using an equation of state explicit in Helmholtz energy. Ancillary equations are given for the ideal gas heat capacity, the vapor pressure, and for the saturated liquid and vapor densities as functions of temperature. Comparisons to available experimental data are given that establish the accuracy of calculated properties using this equation of state. The estimated uncertainties of properties calculated using the new equation are 0.1% in density, 0.5% in heat capacities, 0.02% in the speed of sound for the vapor at pressures less than 1 MPa, 0.5% in the speed of sound elsewhere, and 0.1% in vapor pressure, except in the critical region. The equation is valid for temperatures from the triple point temperature (161.34 K) to 450 K and pressures up to 50 MPa, and can be extrapolated to 650 K. It has been accepted as an international standard formulation for the properties of R-143a by the International Energy Agency-Annex 18. [S0047-2689(00)00404-9]

Key words: caloric properties; density; equation of state; fundamental equation; HFC-143a; R-143a; thermodynamic properties; 1,1,1-trifluoroethane.

Contents

List of Tables

[a)]Electronic mail: ericl@boulder.nist.gov

List of Figures

List of Symbols

Symbol	Physical quantity	Unit
a	Helmholtz energy	J/mol
B	Second virial coefficient	dm^3/mol
C	Third virial coefficient	$(dm^3/mol)^2$
c_p	Isobaric heat capacity	J/(mol·K)
c_v	Isochoric heat capacity	J/(mol·K)
c_σ	Saturated liquid heat capacity	J/(mol·K)
g	Gibbs energy	J/mol
h	Enthalpy	J/mol
M	Molar mass	g/mol
p	Pressure	MPa
R	Molar gas constant	J/(mol·K)
s	Entropy	J/(mol·K)
T	Temperature	K
u	Internal energy	J/mol
v	Molar volume	dm^3/mol
w	Speed of sound	m/s
Z	Compressibility factor ($Z=p/\rho RT$)	
α	Reduced Helmholtz energy ($\alpha=a/RT$)	
δ	Reduced density ($\delta=\rho/\rho_c$)	
ϕ	Fugacity coefficient	
ρ	Molar density	mol/dm^3
τ	Inverse reduced temperature ($\tau=T_c/T$)	

Superscripts

0	Ideal gas property
r	Residual
$'$	Saturated liquid state
$''$	Saturated vapor state

Subscripts

0	Reference state property
c	Critical point property
calc	Calculated using an equation
data	Experimental value
l	Liquid property
nbp	Normal boiling point property
tp	Triple point property
v	Vapor property
σ	Saturation property

Physical Constants and Characteristic Properties of R-143a

Symbol	Quantity	Value
R	Molar gas constant	8.314 472 J/(mol·K)
M	Molar mass	84.041 g/mol
T_c	Critical temperature	345.857 K
p_c	Critical pressure	3.761 MPa
ρ_c	Critical density	5.128 45 mol/dm^3
$T_{\rm tp}$	Triple point temperature	161.34 K
$p_{\rm tp}$	Triple point pressure	0.001 077 MPa
$\rho_{\rm tpv}$	Vapor density at the triple point	0.000 80 mol/dm^3
$\rho_{\rm tpl}$	Liquid density at the triple point	15.83 mol/dm^3
$T_{\rm nbp}$	Normal boiling point temperature	225.91 K
$\rho_{\rm nbpv}$	Vapor density at the normal boiling point	0.0567 mol/dm^3
$\rho_{\rm nbpl}$	Liquid density at the normal boiling point	13.88 mol/dm^3
T_0	Reference temperature	273.15 K
p_0	Reference pressure	0.001 MPa
h_0^0	Reference ideal gas enthalpy at T_0	33 936.4 J/mol
s_0^0	Reference ideal gas entropy at T_0 and p_0	198.961 J/(mol·K)

1. Introduction

Refrigerant 143a (1,1,1-trifluoroethane, HFC-143a), and more importantly blends containing R-143a, are leading candidates for replacing the ozone-depleting hydrochlorofluorocarbon R-22 (chlorodifluoromethane, HCFC-22), the production of which will be phased out by the year 2020 under the terms of the Montreal Protocol. The thermodynamic properties of the refrigerant used as the working fluid in a system significantly influence the energy efficiency and capacity of refrigeration equipment, and accurate properties are thus essential in evaluating potential alternative refrigerants and in designing equipment.

A property formulation is the set of equations used to calculate properties of a fluid at specified thermodynamic states defined by an appropriate number of independent variables. A typical thermodynamic property formulation is based on an equation of state which allows the correlation and computation of all thermodynamic properties of the fluid, including properties such as entropy that cannot be measured directly.

In this work, the general term ''equation of state'' refers to the empirical models developed for calculating fluid thermodynamic properties. The term ''fundamental equation'' is often used in the literature to refer to empirical descriptions of one of four fundamental relations: internal energy as a function of volume and entropy, enthalpy as a function of pressure and entropy, Gibbs energy as a function of pressure and temperature, and Helmholtz energy as a function of density and temperature. Modern equations of state for pure fluid properties are usually fundamental equations explicit in the Helmholtz energy as a function of density and temperature. All thermodynamic properties may be calculated without additional ancillary equations for saturation properties through the use of the Maxwell criterion (equal pressures and Gibbs energies at constant temperature during phase changes).

Several equations of state for R-143a have been developed by various researchers worldwide. The equation of Li *et al.* (1999) is a 19 term equation explicit in the Helmholtz energy, the equation of Piao *et al.* (1998) is an 18 term modified Benedict–Webb–Rubin equation, the equation of Outcalt and McLinden (1997) is a 32 term modified Benedict–Webb–Rubin equation, and the equation presented here, referred to as the Lemmon–Jacobsen equation, is a 17 term fundamental equation explicit in the Helmholtz energy. In view of the importance of R-143a and the existence of several formulations, it was desirable to select an international standard formulation for use by the refrigeration industry. This task was accomplished by a group working under the auspices of the Heat Pump Programme of the International Energy Agency (IEA). The IEA Heat Pump Programme was established in 1978 and is currently supported by 15 countries. It offers opportunities for international collaboration in research, development, demonstration, and promotion of heat pumping and related technologies. Eight member countries (Austria, Canada, Germany, Japan, Norway, Sweden, the United Kingdom, and the United States) joined together to form Annex 18-Thermophysical Properties of the Environmentally Acceptable Refrigerants. One of the goals of this Annex (or Programme project) was to recommend property formulations as international standards for the most important alternative refrigerants and blends.

The comparison and evaluation of the available equations of state for R-143a were assigned by Annex 18 to independent evaluators, namely Yukihiro Higashi of the Iwaki Meisei University and Yoshinori Takaishi of the Kanagawa Institute of Technology, both in Japan. Professor Higashi presented their evaluation at the June, 1998 meeting of Annex 18 in Trondheim, Norway. This evaluation followed the same general procedures as the earlier evaluations for R-123 and R-134a, which are described by Penoncello *et al.* (1995) and for R-32 and R-125 which are described by Kilner and Craven (1997). These earlier evaluations of the IEA-Annex 18 resulted in the designation of international standard for-

mulations for R-134a (Tillner-Roth and Baehr, 1994), R-123 (Younglove and McLinden, 1994), R-32 (Tillner-Roth and Yokozeki, 1997), and R-125 (Piao and Noguchi, 1998). Since that time, the equation of Sunaga *et al.* (1998) for R-125 has been developed which provides improved accuracies in the thermodynamic properties. The Annex has also published a report describing and comparing four mixture models for R-32, R-125, and R-134a, and which is available from the IEA Heat Pump Centre (Lemmon, 1998).

In the evaluation of Higashi and Takaishi, the equations of Li *et al.* and of Lemmon and Jacobsen were shown to be nearly equivalent in their representation of the experimental data for R-143a. The differences between the equations were discussed at the Trondheim meeting, and the final decision of the Annex was made based on these differences. The equation of state of Lemmon and Jacobsen was selected as the international standard for R-143a. However, the two formulations are substantially equivalent, and the Annex felt that either equation was acceptable for analysis or design with very little difference in calculated properties. The final decision was based largely on the vapor pressure comparisons at low temperatures, as discussed in Sec. 4.1. The other major difference between the equations was simply a matter of fitting philosophy. The equation of Li *et al.* tended to fit the average of the more accurate data sets, whereas the equation of Lemmon and Jacobsen tended to fit only one data set in each region.

The equation presented here represents all the selected experimental data within the estimated experimental uncertainties. To minimize the number of coefficients, the new equation of state for R-143a was developed using state of the art optimization and multiproperty fitting algorithms. The equation of state developed in this work is explicit in the reduced Helmholtz energy. Other thermodynamic properties are derived from the equation of state by differentiation. The range of validity of the equation of state for R-143a is from the triple point temperature (161.34 K) to 450 K at pressures to 50 MPa. It can be extrapolated to 650 K based on graphical verification of derived properties.

In addition to the equation of state, ancillary functions are given for the vapor pressure and the density of the saturated liquid and saturated vapor. These ancillary equations can be used as initial estimates in routines that solve for the saturation boundaries, but are not required to calculate properties from the equation of state. Summaries of the available data for the properties of R-143a are given, and the ranges of these data are tabulated.

2. Vapor–Liquid Coexistence

2.1. Critical Point

Critical parameters for R-143a have been reported by various authors and are listed in Table 1. The difficulties in the experimental determination of the critical parameters are the probable cause of considerable differences among the results obtained by the various investigators. The critical density is difficult to determine accurately by experiment because of the infinite compressibility at the critical point and the associated difficulty of reaching thermodynamic equilibrium. Therefore, reported values for the critical density are generally calculated by power-law equations, extrapolation of rectilinear diameters using measured saturation densities, or by correlating single-phase data close to the critical point. The critical temperature used in this work was obtained by fitting the data of Aoyama *et al.* (1996) and Higashi and Ikeda (1996) at temperatures above 333 K to the equation

TABLE 1. Summary of critical point data

Author	Critical temp. (K)	Critical pressure (MPa)	Critical density (kg/m^3)	Critical density (mol/dm^3)
Aoyama *et al.* (1996)	345.86		434	5.164 15
Arnaud *et al.* (1991)	346.00	3.758	455	5.414 02
Fujiwara *et al.* (1998)	345.861	3.7639	434	5.164 15
Fukushima (1993)	345.97	3.769	429	5.104 65
Higashi and Ikeda (1996)	345.88	3.764	431	5.128 45
Mears *et al.* (1955)	346.22	3.758	434	5.164 15
Nagel and Bier (1996)	345.75	3.765	427	5.080 85
Schmidt *et al.* (1996)	346.04		432.9	5.151 06
Wang *et al.* (1993)	346.18	3.780	442	5.259 34
Selected Value	**345.857**	**3.761**	**431**	**5.128 45**

$$\frac{\rho_\sigma}{\rho_c} - 1 = N_1\left(1 - \frac{T_\sigma}{T_c}\right) \pm N_2\left(1 - \frac{T_\sigma}{T_c}\right)^\beta, \tag{1}$$

where $T_c = 345.857$ K, $\rho_c = 5.128\,45$ mol/dm^3, $N_1 = 1.1018$, $N_2 = 1.9755$, $\beta = 0.336$, T_σ is the saturation temperature, and ρ_σ is the saturation density for the liquid or the vapor. The critical density was fixed at the value given by Higashi and Ikeda (1996) and the critical temperature was fitted simultaneously with the coefficients of the equation. Equation (1) is only valid in the critical region. Calculated values from this equation are shown in Fig. 1 along with experimental data along the saturation lines in the critical region. The resulting values of the critical temperature and density and the value of the critical pressure obtained in Sec. 2.2 are

$$T_c = 345.857 \pm 0.015\ \text{K},$$
$$\rho_c = 5.128\ 45\ \text{mol/dm}^3, \tag{2}$$

and

$$p_c = 3.761 \pm 0.004\ \text{MPa}.$$

The experimental value of the critical density, taken from Higashi and Ikeda, was reported as 431 ± 3 kg/m^3. Several additional digits (in the molar value) have been maintained in this work to ensure consistency between the two numbers. The value given in Eq. (2) should be used for all property calculations from the equation of state. The critical temperature agrees well with the values reported by both Aoyama *et al.* (345.86 K) and Higashi and Ikeda (345.88 K).

2.2. Triple Point

The triple point temperature of R-143a was measured by Magee (1998b) by slowly applying a constant heat source to

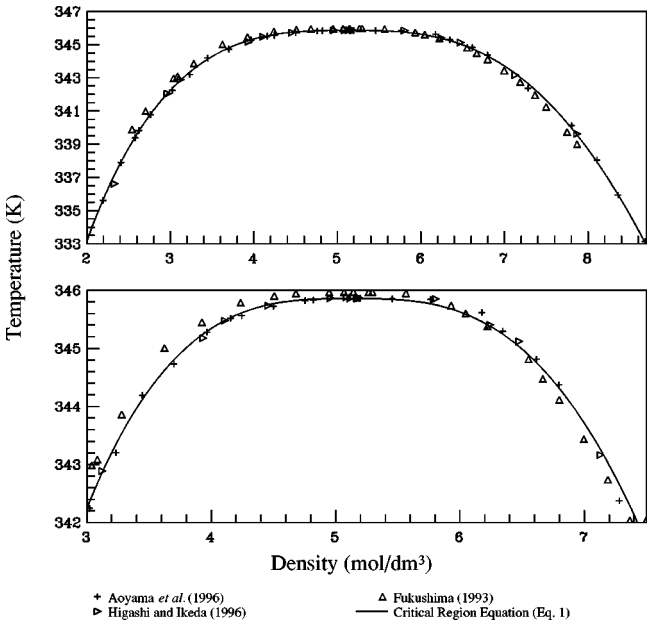

FIG. 1. Critical region saturation data.

a frozen sample and noting the sharp break in the temperature rise. The triple point temperature was also measured by Russell *et al.* (1944) and differs from the result of Magee by 0.48 K. The value of Magee selected in this work is

$$T_{\mathrm{tr}} = 161.34 \pm 0.03\ \mathrm{K}, \tag{3}$$

measured on the ITS-90 temperature scale. The estimated vapor pressure at the triple point derived in the work of Duarte-Garza and Magee (1999) is

$$p_{\mathrm{tr}} = 1.077\ \mathrm{kPa}. \tag{4}$$

This value (and other values of the vapor pressure from Duarte-Garza and Magee used in the following section) was evaluated from measured internal energy changes in the liquid–vapor two-phase region by the use of a thermodynamic relation between the vapor pressure, its derivative with respect to temperature, and the derivative of the internal energy with respect to volume. For comparison, the value of the triple point pressure calculated from the ancillary equation given in the next section is 1.075 kPa.

2.3. Vapor Pressure

Table 2 summarizes the available vapor pressure data for R-143a. The vapor pressure can be represented with the ancillary equation

$$\ln\left(\frac{p_\sigma}{p_c}\right) = \frac{T_c}{T}\left[N_1\tau + N_2\tau^{1.5} + N_3\tau^2 + N_4\tau^{3.5} + N_5\tau^{5.5}\right], \tag{5}$$

where $N_1 = -7.3526$, $N_2 = 1.9162$, $N_3 = -1.2203$, $N_4 = -2.0532$, $N_5 = -1.7354$, $\tau = (1 - T/T_c)$, and p_σ is the vapor pressure. The values of the critical parameters are given in Sec. 2.1. The critical pressure was determined from the regression analysis used to develop Eq. (5). Comparisons

TABLE 2. Summary of vapor pressure data

Author	No. of points	Temp. range (K)	AAD (%)
de Vries (1997)[a]	59	222–345	0.06
Doering *et al.* (1994)	31	198–344	0.33
Duarte-Garza and Magee (1999)[a]	15	161–230	0.07
Fujimine *et al.* (1999)	14	250–330	0.18
Fujiwara and Piao (1995)	23	263–345	0.18
Fujiwara *et al.* (1998)	13	263–345	0.08
Fukushima (1993)	17	275–346	0.11
Giuliani *et al.* (1994)	61	244–346	0.09
Giuliani *et al.* (1995)	33	244–345	0.12
Kubota *et al.* (1990)	4	273–338	0.21
Magee (1998b)	13	165–225	0.13
Mears *et al.* (1955)	7	226–345	0.44
Nagel and Bier (1996)	26	205–346	0.32
Russell *et al.* (1944)	9	174–226	0.28
Takashima and Higashi (1995)	12	273–333	0.19
Tsuge *et al.* (1997)	31	300–346	0.14
Wang *et al.* (1993)	30	312–346	0.06
Weber and Defibaugh (1996)[a]	52	236–343	0.03
Widiatmo *et al.* (1994)	12	280–340	0.41
Ye (1994)	11	310–342	0.41
Zhang *et al.* (1995)	11	295–342	0.20
Overall	484	161–346	0.15

[a]Data used in the development of the ancillary equation.

of values calculated using this equation to the vapor pressure data are given in Fig. 2. The bottom plot of this figure shows selected data on an expanded scale. The equation best represents the data of Duarte-Garza and Magee (1999) between the triple point temperature and 230 K, the data of Weber

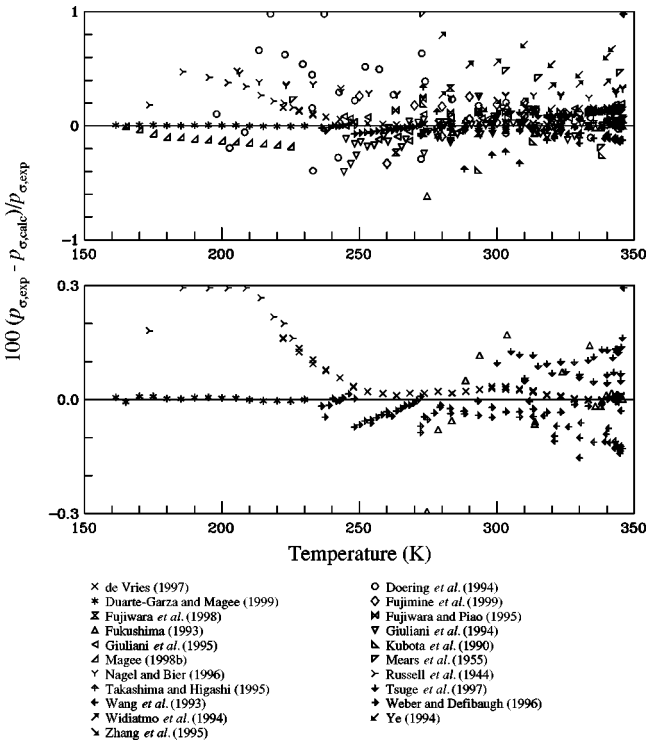

FIG. 2. Comparisons of vapor pressures calculated with the ancillary equation to experimental data.

TABLE 3. Summary of saturated liquid and vapor density data

Author	No. of points	Temp. range (K)	AAD (%)
Saturated liquid density data			
Aoyama *et al.* (1996)[a]	15	333–346	1.34
Defibaugh and Moldover (1997)	20	245–340	0.22
Doering *et al.* (1994)	4	276–283	2.19
Fujimine *et al.* (1999)	14	250–330	0.33
Fukushima (1993)	16	339–346	0.94
Higashi and Ikeda (1996)[a]	7	340–346	2.07
Magee (1998a)[a]	8	164–298	0.11
Mears *et al.* (1955)	6	298–338	3.44
Widiatmo *et al.* (1994)	17	230–340	0.54
Yokoyama and Takahashi (1991)	16	248–341	0.30
Overall	123	164–346	0.80
Saturated vapor density data			
Aoyama *et al.* (1996)[a]	20	336–346	1.45
Fukushima (1993)	12	340–346	4.96
Higashi and Ikeda (1996)[a]	8	337–346	0.81
Overall	40	336–346	2.16

[a]Data used in the development of the ancillary equations.

and Defibaugh (1996) between 236 and 248 K, and the data of de Vries (1997) between 252 K and the critical point temperature. Below 248 K, the data of de Vries deviate from the data of Weber and Defibaugh and of Duarte-Garza and Magee by as much as 0.16%, but are in good agreement with the older data of Russell *et al.* (1944). Furthermore, the differences tend to increase at lower temperatures between the data of Russell *et al.* and of Duarte-Garza and Magee and reach a maximum of 0.47% at 186 K. Above 300 K, the data of de Vries (1997), Fukushima (1993), Tsuge *et al.* (1997), Wang *et al.* (1993), and Weber and Defibaugh (1996) generally agree within 0.1%.

2.4. Saturated Densities

Table 3 summarizes the saturated liquid and vapor density data for R-143a. The saturated liquid density is represented by the ancillary equation

$$\frac{\rho'}{\rho_c} = 1 + N_1\tau^{1/3} + N_2\tau^{2/3} + N_3\tau^{8/3}, \tag{6}$$

where $N_1 = 1.795$, $N_2 = 0.8709$, $N_3 = 0.3116$, $\tau = (1 - T/T_c)$, and ρ' is the saturated liquid density. Deviations of saturated liquid density values calculated using this equation from experimental values are given in Fig. 3. The data of Magee (1998a) were used to develop Eq. (6), and both the data of Magee and of Defibaugh and Moldover (1997) are represented within 0.1% in density at temperatures below 330 K. Differences between various data sets are significantly higher than is generally expected for saturated liquid densities as shown in Fig. 3. However, the data of Magee tend to agree well with the single phase liquid $p\rho T$ data presented in the following sections.

The saturated vapor density is represented by the equation

$$\ln\left(\frac{\rho''}{\rho_c}\right) = N_1\tau^{0.39} + N_2\tau^{4/3} + N_3\tau^{11/3} + N_4\tau^{23/3}, \tag{7}$$

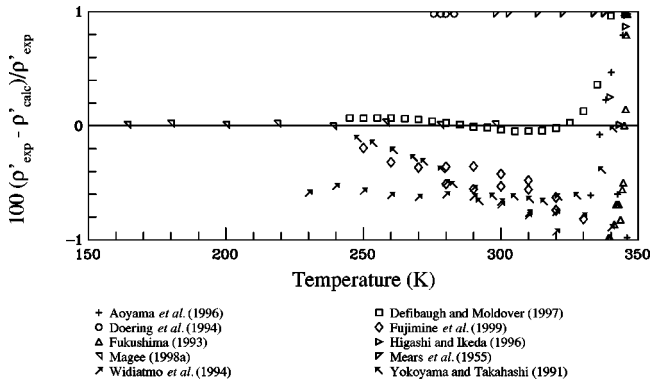

FIG. 3. Comparisons of saturated liquid densities calculated with the ancillary equation to experimental data.

where $N_1 = -3.072$, $N_2 = -8.061$, $N_3 = -23.74$, $N_4 = -61.37$, and ρ'' is the saturated vapor density. Since experimental values for the saturated density are available only at temperatures above 335 K, additional vapor density data used to develop Eq. (7) were calculated from the equation of state presented in the next section at various temperatures along the saturation line using the Maxwell criterion. Deviations of saturated density values in the critical region calculated using Eqs. (6) and (7) from experimental values are given in Fig. 4. Deviations between values calculated from these equations and from Eq. (1) are also shown in this figure.

3. The Equation of State for R-143a

The equation of state for R-143a has been formulated using the Helmholtz energy as the fundamental property with independent variables of density and temperature. The equation of state is given by

$$a(\rho,T) = a^0(\rho,T) + a^r(\rho,T), \tag{8}$$

where a is the Helmholtz energy, $a^0(\rho,T)$ is the ideal gas contribution to the Helmholtz energy, and $a^r(\rho,T)$ is the residual Helmholtz energy which corresponds to the influ-

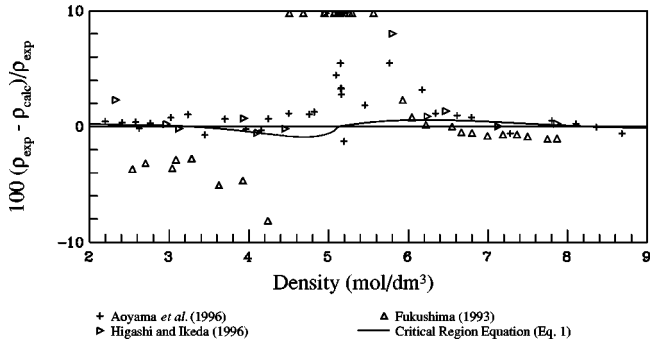

FIG. 4. Comparisons of saturated liquid and vapor densities in the critical region calculated with the ancillary equations to experimental data.

ence of intermolecular forces. All thermodynamic properties can be calculated as derivatives of the Helmholtz energy. For example, the pressure derived from this expression is

$$p=\rho^2\left(\frac{\partial a}{\partial \rho}\right)_T. \tag{9}$$

The functional form used for the new equation for R-143a is explicit in the dimensionless Helmholtz energy, α, using independent variables of dimensionless density and temperature. The form of this equation is

$$\frac{a(\rho,T)}{RT}=\alpha(\delta,\tau)=\alpha^0(\delta,\tau)+\alpha^r(\delta,\tau), \tag{10}$$

where $\delta=\rho/\rho_c$, $\tau=T_c/T$, the critical temperature (T_c) is 345.857 K, and the critical density (ρ_c) is 5.128 45 mol/dm^3 as given in Sec. 2.1. The equation for the ideal gas Helmholtz energy is given in Sec. 3.1 and the equation for the residual Helmholtz energy is given in Sec. 3.2.3.

3.1. Properties of the Ideal Gas

The Helmholtz energy of the ideal gas is given by

$$a^0=h^0-RT-Ts^0. \tag{11}$$

The ideal gas enthalpy is given by

$$h^0=h_0^0+\int_{T_0}^{T}c_p^0 dT, \tag{12}$$

where $h_0^0=33\,936.4$ J/mol is the value at $T_0=273.15$ K, and c_p^0 is the ideal gas heat capacity given by Eq. (16) below. The ideal gas entropy is given by

$$s^0=s_0^0+\int_{T_0}^{T}\frac{c_p^0}{T}dT-R\ln\left(\frac{\rho T}{\rho_0 T_0}\right), \tag{13}$$

where $s_0^0=198.961$ J/(mol·K) is the value for entropy at $T_0=273.15$ K and $p_0=0.001$ MPa, and ρ_0 is the ideal gas density at T_0 and p_0. The values for h_0^0 and s_0^0 were chosen so that the enthalpy and entropy of the saturated liquid state at 0 °C are 200 kJ/kg and 1 kJ/(kg·K), respectively, corresponding to the common convention in the refrigeration industry. Combining these equations results in the following equation for the Helmholtz energy of the ideal gas

$$a^0=h_0^0+\int_{T_0}^{T}c_p^0\,dT-RT-T\times\left[s_0^0+\int_{T_0}^{T}\frac{c_p^0}{T}dT-R\ln\left(\frac{\rho T}{\rho_0 T_0}\right)\right]. \tag{14}$$

The ideal gas Helmholtz energy is given in a dimensionless form by

$$\alpha^0=\frac{h_0^0\tau}{RT_c}-\frac{s_0^0}{R}-1+\ln\frac{\delta\tau_0}{\delta_0\tau}-\frac{\tau}{R}\int_{\tau_0}^{\tau}\frac{c_p^0}{\tau^2}d\tau+\frac{1}{R}\int_{\tau_0}^{\tau}\frac{c_p^0}{\tau}d\tau, \tag{15}$$

where $\delta_0=\rho_0/\rho_c$ and $\tau_0=T_c/T_0$.

TABLE 4. Summary of ideal gas heat capacity data

Author	No. of points	Temp. range (K)	AAD (%)
Experimental Data			
Beckermann and Kohler (1995)	18	250–410	0.47
Gillis (1997)	8	250–400	0.14
Ogawa and Sato (1999)	5	303–343	0.03
Vanderkooi and de Vries (1956)	1	300	0.42
Overall	32	250–410	0.32
Calculated Values			
Chen *et al.* (1975)	18	100–1500	0.63
Mears *et al.* (1955)	9	200–1000	1.67
Smith *et al.* (1952)	4	250–600	0.69
Yokozeki *et al.* (1998)	45	120–1000	0.02

In the calculation of the thermodynamic properties of R-143a using an equation of state explicit in the Helmholtz energy, an equation for the ideal gas heat capacity, c_p^0, is needed to calculate the Helmholtz energy for the ideal gas, α^0. Values of the ideal gas heat capacity derived from low pressure experimental heat capacity or speed of sound data are given in Table 4 along with calculated values from statistical methods using fundamental frequencies. Differences between the calculated values arise from the use of different fundamental frequencies and from the models used to calculate the various couplings between the vibrational modes of the molecule. The equation for the ideal gas heat capacity for R-143a, used throughout the remainder of this work, was developed by fitting values reported by Yokozeki *et al.* (1998), and is given by

$$\frac{c_p^0}{R}=1.0578T^{0.33}+4.4402\,\frac{u_1^2\exp(u_1)}{[\exp(u_1)-1]^2}+3.7515\,\frac{u_2^2\exp(u_2)}{[\exp(u_2)-1]^2}, \tag{16}$$

where u_1 is 1791 K/T, u_2 is 823 K/T, and the ideal gas constant, R, is 8.314 472 J/(mol·K) (Mohr and Taylor, 1999). The Einstein functions containing the terms u_1 and u_2 were used so that the shape of the ideal gas heat capacity with respect to temperature would be similar to that derived from statistical methods, however, the empirical coefficients in u_1 and u_2 should not be used to calculate the fundamental frequencies. Comparisons of values calculated using Eq. (16) to the ideal gas heat capacity data are given in Fig. 5. The ideal gas Helmholtz energy equation, derived from Eqs. (15) and (16), is

$$\alpha^0=\ln\delta-\ln\tau+a_1+a_2\tau+a_3\tau^{-0.33}+a_4\ln[1-\exp(-a_5\tau)]+a_6\ln[1-\exp(-a_7\tau)], \tag{17}$$

where $a_1=5.903\,087$, $a_2=7.307\,253$, $a_3=-16.591\,05$, $a_4=4.4402$, $a_5=5.178\,4408$, $a_6=3.7515$, and $a_7=2.379\,5962$.

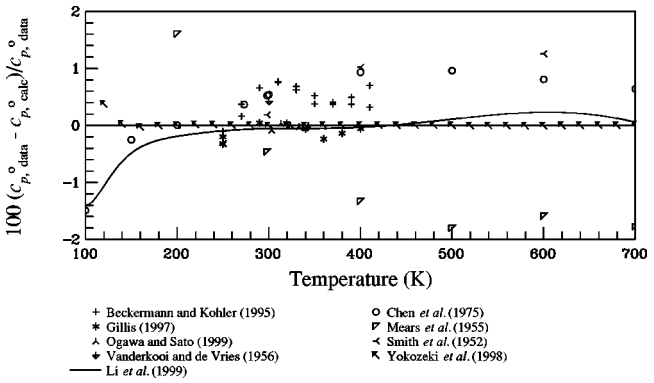

FIG. 5. Comparisons of ideal gas heat capacities calculated with the ancillary equation to experimental and calculated data.

3.2. Properties of the Real Fluid

Unlike the equations for the ideal gas, the nonideal gas, or real fluid, behavior is described using empirical models that are only loosely tied with theoretical techniques. Equations for the second and third virial coefficients can generally be extracted from the fundamental equation, however, the terms in the equation are empirical and are determined by correlation techniques using experimental data. The coefficients of the equation reported here depend solely on the experimental data described in Sec. 4.

3.2.1. Selected Database

The units adopted for this work were K (ITS-90) for temperature, MPa for pressure, and mol/dm^3 for density. Units of the experimental data were converted as necessary from those of the original publications to these units. All temperatures were converted to the International Temperature Scale of 1990 (ITS-90) (Preston-Thomas, 1990).

The $p\rho T$ data selected for the determination of the coefficients of the equation of state are described in Sec. 4. Data used in fitting the equation of state for R-143a were selected to avoid redundancy in various regions of the surface. In total, 835 data points out of the 2811 available for $p\rho T$ data and 86 data points out of the 594 available for speed of sound were used in the nonlinear fitting procedure described in the next section. In addition to these data, 31 isochoric heat capacity data, 5 saturated liquid heat capacity data, and 15 calculated second virial coefficients were used in the fit. Thirteen vapor pressure values were also used in the regression.

3.2.2. Fitting Procedures

The development of the equation of state is a process of correlating selected experimental data by least-squares fitting methods using a model which is generally empirical in nature, but is designed to exhibit proper behavior in the ideal gas and low density regions and to extrapolate to temperatures and pressures higher than those defined by experiment. In all cases, experimental data are considered paramount, and the proof of validity of any equation of state is evidenced in its ability to represent the thermodynamic properties of the fluid within the uncertainty of the experimental values, and in its ability to extrapolate outside the range of experimental data. The selected data are usually a subset of the available database determined by the correlator to be representative of the most accurate values measured. The type of fitting procedure (e.g., nonlinear versus linear) determines how the experimental data will be used. In this work, a much smaller subset of the most accurate data was used in the nonlinear fitting due to the extensive calculations required to develop the equation. The resulting equation was compared to all experimental data to verify that the data reduction had not affected the fit. The data for R143a are discussed in detail in Sec. 4 and comparisons of calculated properties to experimental values are given to verify the accuracy of the model developed in this research.

Two methods were used to arrive at the final equation of state for R-143a. Initial equations were developed using linear regression techniques by fitting $p\rho T$ data, isochoric heat capacity data, linearized sound speed data, and second virial coefficients, as well as vapor pressures calculated from the ancillary equation. This process has been widely used to develop equations of state over the last several decades and typically results in equations with 28–35 terms. In this work, the best equation developed from the linear regression was used as the starting point for the second method discussed below. Details about the liear regression algorithm can be found elsewhere (Wagner, 1974; Lemmon *et al.*, 2000).

Once a preliminary equation had been developed, nonlinear fitting techniques were used to shorten and improve the equation. Only a subset of the primary data was used. The nonlinear algorithm adjusted the coefficients of the equation of state to reduce the overall sum of squares of the deviations of calculated properties from the input data. Each data point was individually weighted according to type, region, and uncertainty. The values of the first and second derivatives of pressure with respect to density at the critical point were fitted so that their values would be near zero at the selected critical point given in Sec. 2.1. In addition, the exponents for density and temperature, given below in Eq. (18) as i_k and j_k, were also determined simultaneously with the coefficients of the equation. To reduce the size of the equation, terms were eliminated by either deleting the term that contributed least to the overall sum of squares or by combining two terms that had similar functional forms (similar contributions to the equation of state). After a term was eliminated, the fit was rerun until the sum of squares with the new equation was of the same magnitude as the previous equation. The final functional form resulted in an equation with 17 terms.

The exponents on density in the equation of state must be integers so that the derivatives of the Helmholtz energy with respect to density are zero in the ideal gas limit. Since noninteger values for the density exponents resulted from the nonlinear fitting, a process of rounding a density exponent to the nearest integer, followed by refitting the other parameters to minimize the overall sum of squares, was implemented

TABLE 5. Parameters and coefficients of the equation of state

k	N_k	i_k	j_k	l_k
1	7.773 644 3	1	0.67	
2	−8.701 850 0	1	0.833	
3	−0.277 797 99	1	1.7	
4	0.146 092 20	2	1.82	
5	0.008 958 161 6	5	0.35	
6	−0.205 521 16	1	3.9	1
7	0.106 532 58	3	0.95	1
8	0.023 270 816	5	0.0	1
9	−0.013 247 542	7	1.19	1
10	−0.042 793 870	1	7.2	2
11	0.362 216 85	2	5.9	2
12	−0.256 718 99	2	7.65	2
13	−0.092 326 113	3	7.5	2
14	0.083 774 837	4	7.45	2
15	0.017 128 445	2	15.5	3
16	−0.017 256 110	3	22.0	3
17	0.004 908 049 2	5	19.0	3

until all the exponents were integers. A similar process was used for the temperature exponents to reduce the number of significant figures to one or two digits past the decimal point. The final equation with 17 terms represented the experimental data better than preliminary equations resulting from the linear fitter with about 32 terms.

In addition to reducing the number of individual terms in the equation compared to that produced by conventional linear least-squares methods, the extrapolation behavior of the shorter equations will generally be more accurate because there are less degrees of freedom. In the longer equations, two or more correlated terms are often needed to reproduce the accuracy of a single term in the nonlinear fit. The values of these correlated terms are often large in magnitude, and their behavior outside the range of validity of the equation is often unreasonable.

3.2.3. Equation for the Residual Helmholtz Energy

The original equation presented to the IEA Annex-18 was a 20 term Helmholtz equation with a critical temperature of 345.88 K. Further analysis of the equation after the Annex meeting showed an anomaly in the ideal Joule inversion curve (given in Sec. 4.4) which was caused in part by two of the terms in the equation with negative exponents on τ. Such terms are quite common in typical equations of state but they often cause extrapolation problems at high temperatures $(T/T_c > 5)$. Additional analysis of the critical region saturated density data showed that the selected critical temperature for the preliminary equation was slightly too high, and that the value of 345.857 K gave better results (see Fig. 1). Thus, the equation was further optimized with a new T_c, and the anomalous behavior of the ideal Joule inversion curve was eliminated. In addition, the number of terms in the final equation was reduced from 20 to 17. The accuracy of properties calculated using the final equation is equivalent to that of the preliminary equation presented to the IEA Annex-18.

The final functional form for the residual Helmholtz energy for R-143a is

$$\alpha^r(\delta,\tau)=\sum_{k=1}^{5} N_k \delta^{i_k}\tau^{j_k}+\sum_{k=6}^{17} N_k \delta^{i_k}\tau^{j_k}\exp(-\delta^{l_k}). \tag{18}$$

The coefficients N_k of this equation are given in Table 5. Although the values of i_k, j_k, and l_k are arbitrary, j_k is generally expected to be greater than zero, and i_k and l_k are integers greater than zero.

The functions used for calculating pressure, compressibility factor, internal energy, enthalpy, entropy, Gibbs energy, isochoric heat capacity, isobaric heat capacity, and the speed of sound from Eq. (10) are given as Eqs. (19)–(27). These equations were used in calculating the tables of thermodynamic properties of R-143a given in the Appendix.

$$p=\rho RT\left[1+\delta\left(\frac{\partial\alpha^r}{\partial\delta}\right)_\tau\right] \tag{19}$$

$$Z=\frac{p}{\rho RT}=1+\delta\left(\frac{\partial\alpha^r}{\partial\delta}\right)_\tau \tag{20}$$

$$\frac{u}{RT}=\tau\left[\left(\frac{\partial\alpha^0}{\partial\tau}\right)+\left(\frac{\partial\alpha^r}{\partial\tau}\right)_\delta\right] \tag{21}$$

$$\frac{h}{RT}=\tau\left[\left(\frac{\partial\alpha^0}{\partial\tau}\right)_\delta+\left(\frac{\partial\alpha^r}{\partial\tau}\right)_\delta\right]+\delta\left(\frac{\partial\alpha^r}{\partial\delta}\right)_\tau+1 \tag{22}$$

$$\frac{s}{R}=\tau\left[\left(\frac{\partial\alpha^0}{\partial\tau}\right)_\delta+\left(\frac{\partial\alpha^r}{\partial\tau}\right)_\delta\right]-\alpha^0-\alpha^r \tag{23}$$

$$\frac{g}{RT}=1+\alpha^0+\alpha^r+\delta\left(\frac{\partial\alpha^r}{\partial\delta}\right)_\tau \tag{24}$$

$$\frac{c_v}{R}=-\tau^2\left[\left(\frac{\partial^2\alpha^0}{\partial\tau^2}\right)_\delta+\left(\frac{\partial^2\alpha^r}{\partial\tau^2}\right)_\delta\right] \tag{25}$$

$$\frac{c_p}{R}=\frac{c_v}{R}+\frac{\left[1+\delta\left(\frac{\partial\alpha^r}{\partial\delta}\right)_\tau-\delta\tau\left(\frac{\partial^2\alpha^r}{\partial\delta\partial\tau}\right)\right]^2}{\left[1+2\delta\left(\frac{\partial\alpha^r}{\partial\delta}\right)_\tau+\delta^2\left(\frac{\partial^2\alpha^r}{\partial\delta^2}\right)_\tau\right]} \tag{26}$$

$$\frac{w^2M}{RT}=1+2\delta\left(\frac{\partial\alpha^r}{\partial\delta}\right)_\tau+\delta^2\left(\frac{\partial^2\alpha^r}{\partial\delta^2}\right)_\tau-\frac{\left[1+\delta\left(\frac{\partial\alpha^r}{\partial\delta}\right)_\tau-\delta\tau\frac{\partial^2\alpha^r}{\partial\delta\partial\tau}\right]^2}{\tau^2\left[\left(\frac{\partial^2\alpha^0}{\partial\tau^2}\right)_\delta+\left(\frac{\partial^2\alpha^r}{\partial\tau^2}\right)_\delta\right]} \tag{27}$$

Equations for the fugacity coefficient and second and third virial coefficients are given in Eqs. (28)–(30).

$$\phi = \exp[Z - 1 - \ln(Z) + \alpha^r] \tag{28}$$

$$B(T) = \frac{1}{\rho_c}\left(\frac{\partial \alpha^r}{\partial \delta}\right)_{\delta=0} \tag{29}$$

$$C(T) = \frac{1}{\rho_c^2}\left(\frac{\partial^2 \alpha^r}{\partial \delta^2}\right)_{\delta=0} \tag{30}$$

Other derived properties, given in Eqs. (31)–(33), include the first derivative of pressure with respect to density ($\partial p/\partial \rho$), the second derivative of pressure with respect to density ($\partial^2 p/\partial \rho^2$), and the first derivative of pressure with respect to temperature ($\partial p/\partial T$).

$$\left(\frac{\partial p}{\partial \rho}\right)_T = RT\left[1 + 2\delta\left(\frac{\partial \alpha^r}{\partial \delta}\right)_\tau + \delta^2\left(\frac{\partial^2 \alpha^r}{\partial \delta^2}\right)_\tau\right] \tag{31}$$

$$\left(\frac{\partial^2 p}{\partial \rho^2}\right)_T = \frac{RT}{\rho}\left[2\delta\left(\frac{\partial \alpha^r}{\partial \delta}\right)_\tau + 4\delta^2\left(\frac{\partial^2 \alpha^r}{\partial \delta^2}\right)_\tau + \delta^3\left(\frac{\partial^3 \alpha^r}{\partial \delta^3}\right)_\tau\right] \tag{32}$$

$$\left(\frac{\partial p}{\partial T}\right)_\rho = R\rho\left[1 + \delta\left(\frac{\partial \alpha^r}{\partial \delta}\right)_\tau - \delta\tau\left(\frac{\partial^2 \alpha^r}{\partial \delta \partial \tau}\right)\right] \tag{33}$$

Equations for additional thermodynamic properties such as the isothermal compressibility and the Joule–Thomson coefficient are given in Lemmon *et al.* (2000).

The derivatives of the ideal gas Helmholtz energy are

$$\frac{\partial \alpha^0}{\partial \tau} = \frac{-1}{\tau} + a_2 - 0.33 a_3 \tau^{-1.33} + a_4 a_5\left[\frac{1}{\exp(a_5\tau) - 1}\right] + a_6 a_7\left[\frac{1}{\exp(a_7\tau) - 1}\right], \tag{34}$$

and

$$\frac{\partial^2 \alpha^0}{\partial \tau^2} = \tau^{-2} + 0.33(1.33) a_3 \tau^{-2.33} - a_4 a_5^2 \frac{\exp(a_5\tau)}{[\exp(a_5\tau) - 1]^2} - a_6 a_7^2 \frac{\exp(a_7\tau)}{[\exp(a_7\tau) - 1]^2}, \tag{35}$$

where a_1 through a_8 are given in Eq. (17). The derivatives of the residual Helmholtz energy are given in Eqs. (36)–(41).

$$\frac{\partial \alpha^r}{\partial \delta} = \sum_{k=1}^{5} i_k N_k \delta^{i_k - 1} \tau^{j_k} + \sum_{k=6}^{17} N_k \delta^{i_k - 1} \tau^{j_k} \times \exp(-\delta^{l_k})(i_k - l_k \delta^{l_k}) \tag{36}$$

$$\frac{\partial^2 \alpha^r}{\partial \delta^2} = \sum_{k=1}^{5} i_k (i_k - 1) N_k \delta^{i_k - 2} \tau^{j_k} + \sum_{k=6}^{17} N_k \delta^{i_k - 2} \tau^{j_k} \times \exp(-\delta^{l_k})[(i_k - l_k \delta^{l_k})(i_k - 1 - l_k \delta^{l_k}) - l_k^2 \delta^{l_k}] \tag{37}$$

$$\frac{\partial^3 \alpha^r}{\partial \delta^3} = \sum_{k=1}^{5} i_k (i_k - 1)(i_k - 2) N_k \delta^{i_k - 3} \tau^{j_k} + \sum_{k=6}^{17} N_k \delta^{i_k - 3} \tau^{j_k} \times \exp(-\delta^{l_k})\{i_k (i_k - 1)(i_k - 2) + \delta^{l_k}[-2l_k + 6 i_k l_k - 3 i_k^2 l_k - 3 i_k l_k^2 + 3 l_k^2 - l_k^3] + \delta^{2 l_k}[3 i_k l_k^2 - 3 l_k^2 + 3 l_k^3] - l_k^3 \delta^{3 l_k}\} \tag{38}$$

$$\frac{\partial \alpha^r}{\partial \tau} = \sum_{k=1}^{5} j_k N_k \delta^{i_k} \tau^{j_k - 1} + \sum_{k=6}^{17} j_k N_k \delta^{i_k} \tau^{j_k - 1} \exp(-\delta^{l_k}) \tag{39}$$

$$\frac{\partial^2 \alpha^r}{\partial \tau^2} = \sum_{k=1}^{5} j_k (j_k - 1) N_k \delta^{i_k} \tau^{j_k - 2} + \sum_{k=6}^{17} j_k (j_k - 1) N_k \delta^{i_k} \tau^{j_k - 2} \exp(-\delta^{l_k}) \tag{40}$$

$$\frac{\partial^2 \alpha^r}{\partial \tau \partial \delta} = \sum_{k=1}^{5} i_k j_k N_k \delta^{i_k - 1} \tau^{j_k - 1} + \sum_{k=6}^{17} j_k N_k \delta^{i_k - 1} \tau^{j_k - 1} \times \exp(-\delta^{l_k})(i_k - l_k \delta^{l_k}) \tag{41}$$

4. Experimental Data and Comparisons to the Equation of State

During the last several years, many experimental studies of the thermodynamic properties of R-143a have been reported, e.g., $p\rho T$ properties, saturation properties, critical parameters, heat capacities, speeds of sound, second virial coefficients, and ideal gas heat capacities. Selected data were used for the development of the new thermodynamic property formulation reported here. Comparisons were made to all available experimental data, including those not used in the development of the equation of state. The data for the coexistence states are discussed and summarized in Sec. 2.

The accuracy of the equation of state was determined by statistical comparisons of property values calculated using the equation of state to experimental data. These statistics are based on the percent deviation in any property X defined as

$$\%\Delta X = 100\left(\frac{X_{\text{data}} - X_{\text{calc}}}{X_{\text{data}}}\right). \tag{42}$$

Using this definition, the average absolute deviation (AAD) is defined as

$$\text{AAD} = \frac{1}{n}\sum_{i=1}^{n} |\%\Delta X_i|, \tag{43}$$

where n is the number of data points. The average absolute deviations between experimental data and the equation of state are given in the tables summarizing the data. In Tables 2 and 3, measured properties are compared with the equation of state, not with the ancillary equations.

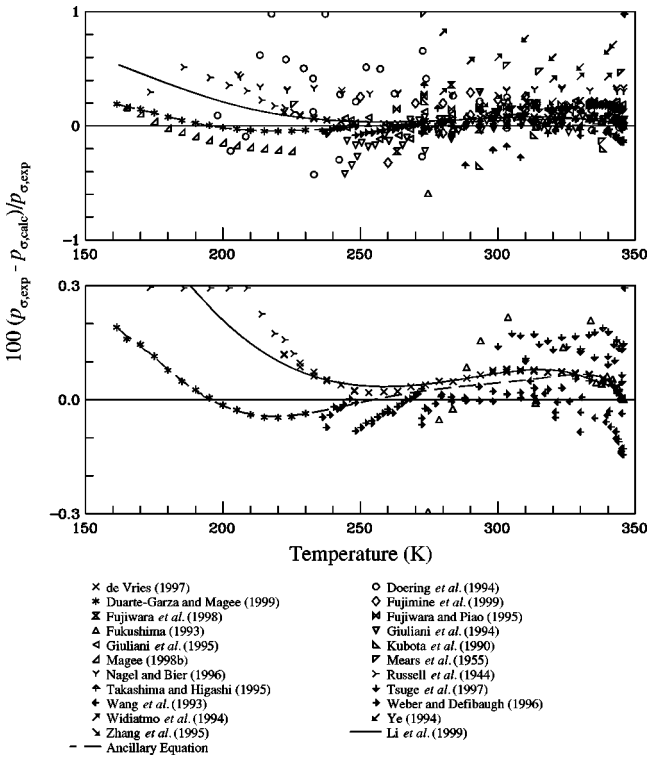

FIG. 6. Comparisons of vapor pressures calculated with the equation of state to experimental data.

4.1. Comparisons with Saturation Data

Figures 6 and 7 show comparisons of vapor pressures calculated from the equation of state with experimental data. The dashed lines in these figures represent the ancillary equation reported in Sec. 2.3. The maximum deviation (at temperatures above 180 K) between the vapor pressure ancillary equation and the equation of state is 0.08%. Near the triple point, the maximum difference is about 0.19%. The average absolute deviation is 0.03% for the data of Weber and Defibaugh (1996), 0.06% for the data of de Vries (1997), and 0.07% for the calculations of Duarte-Garza and Magee (1999). Also shown in Figs. 6 and 7 is the equation by Li *et al.* (1999). This equation is very similar to that presented here at temperatures above 250 K, but tends to follow the

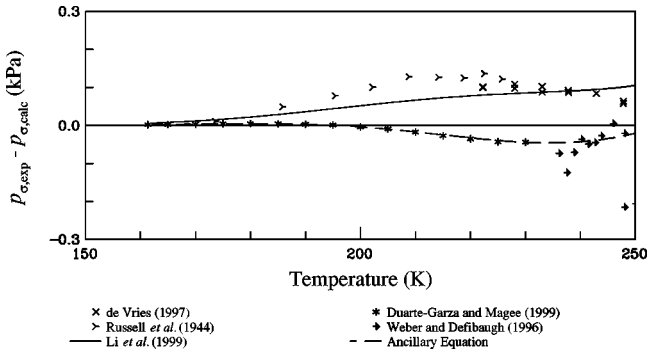

FIG. 7. Comparisons of vapor pressures at low temperatures calculated with the equation of state to experimental data.

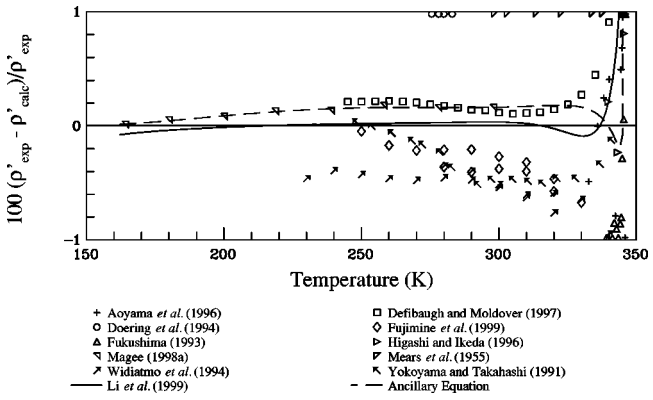

FIG. 8. Comparisons of saturated liquid densities calculated with the equation of state to experimental data.

data of de Vries (1997) and of Russell *et al.* (1944) at lower temperatures. During the course of the IEA Annex-18 meeting in Trondheim to select an international standard for R-143a, this difference was one of the main issues discussed. The final conclusion was that the data of de Vries may have been susceptible to slight impurities and that the accuracy of the historic data of Russell *et al.* could not be verified. The vapor pressure values of Duarte-Garza and Magee (1999) calculated from caloric information in the two-phase region were believed to be the most reliable values available.

Figure 8 shows comparisons of saturated liquid densities calculated from the equation of state with experimental data. Figure 9 shows similar comparisons, but with saturated liquid and vapor densities in the critical region. The dashed lines in these figures represent the ancillary equations reported in Sec. 2.4. There is a large discrepancy between saturated liquid density data at temperatures above 230 K. Excluding the critical region, these differences are as high as $\pm 1\%$. The equation of state tends to split the difference between the experimental data, tending more toward the data of Magee (1998a). There are no saturated vapor density data outside the critical region. In the critical region, the equation of state agrees well with the data of Aoyama *et al.* (1996) and Higashi and Ikeda (1996). The critical point of the equation of state was determined using these data, and the equa-

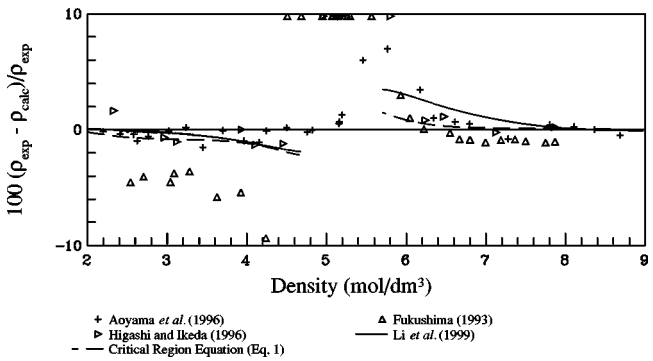

FIG. 9. Comparisons of saturated liquid and vapor densities in the critical region calculated with the equation of state to experimental data.

TABLE 6. Summary of $p\rho T$ data

Source	No. of points	Temp. range (K)	Pressure range (MPa)	Density range (mol/dm^3)	AAD (%)
de Vries (1997)[a]	1062	243–433	0.02–21.	0.01–14.	0.08
Defibaugh and Moldover (1997)	816	243–372	1.50–6.5	2.1–14.	0.26
Fujimine *et al.* (1999)	39	250–330	0.50–3.0	9.1–13.	0.21
Fujiwara and Piao (1995)	40	263–393	0.43–3.5	0.22–1.4	0.45
Giuliani *et al.* (1994)	14	274–364	0.57–0.8	0.29–0.30	0.10
Giuliani *et al.* (1995)	62	268–364	0.50–4.1	0.26–5.1	0.81
Magee (1998a)[a]	144	166–400	3.0–35.	8.5–16.	0.09
Mears *et al.* (1955)	21	320–369	1.3–4.3	0.58–2.7	2.54
Nakamura *et al.* (1997)	215	263–403	1.5–15.	0.48–13.	0.18
Takahashi *et al.* (1999)	97	298–423	0.10–8.8	0.03–4.3	0.42
Tsuge *et al.* (1997)	25	346–433	3.8–11.	5.1–5.2	0.74
Weber and Defibaugh (1996)	117	277–373	0.23–6.6	0.11–6.1	0.07
Ye (1994)	58	300–360	0.14–3.1	0.05–2.0	0.22
Zhang *et al.* (1995)	92	320–380	0.11–6.1	0.04–7.4	0.08
Overall	2802	166–433	0.02–35.	0.01–16.	0.20

[a]Data used in the development of the equation of state.

tion of state was fitted as explained in Sec. 3.2.2 to meet the critical point criteria, resulting in consistency of calculated properties with these two recent data sets. The data of Fukushima (1993) differ significantly from the other two data sets and were not used in the fit.

4.2. $p\rho T$ Data and Virial Coefficients

The experimental $p\rho T$ data for R-143a are summarized in Table 6. The table indicates those data used in the development of the equation of state. Figure 10 shows all available $p\rho T$ data for R-143a. For clarity, data in the critical region are also shown in Fig. 11. The data used to nonlinearly fit the equation of state are shown in Fig. 12. The calculated vapor pressure data shown in the figure and used during fitting were generated from the vapor pressure ancillary equation. Figure 13 shows comparisons of densities calculated from the equation of state with experimental data and Fig. 14 shows comparisons of pressures calculated from the equation of state with the experimental data in the extended critical region of R-143a. The only experimental data in the liquid between the triple point and 240 K are the data of Magee (1998a). Differences between these data and the equation of state are about 0.05% in density near the triple point and 0.12% at 240 K, at which point the data of Magee and of de Vries differ by approximately 0.1%. Between 240 K and the upper limit of the equation, the equation was fitted to the data of de Vries with an average absolute deviation of 0.08%

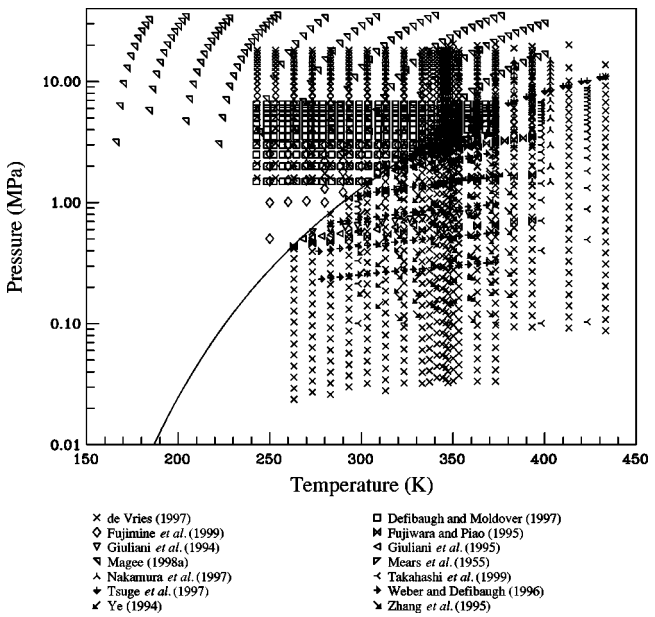

FIG. 10. Experimental $p\rho T$ data.

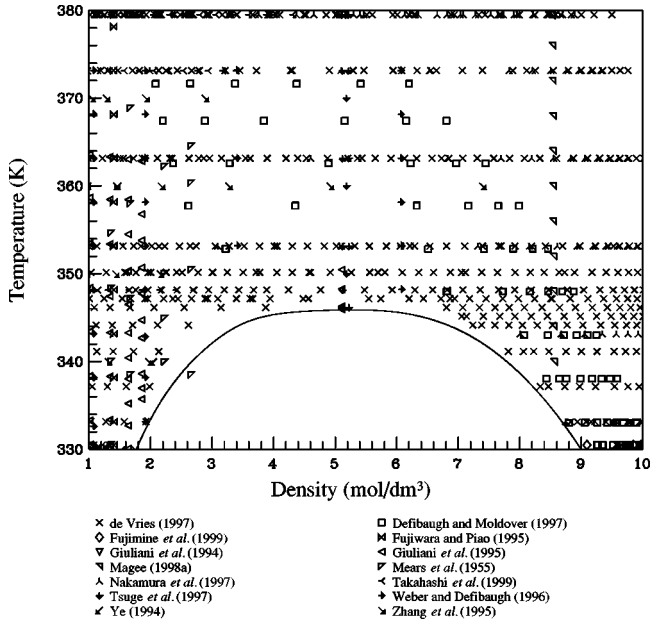

FIG. 11. Critical region $p\rho T$ data.

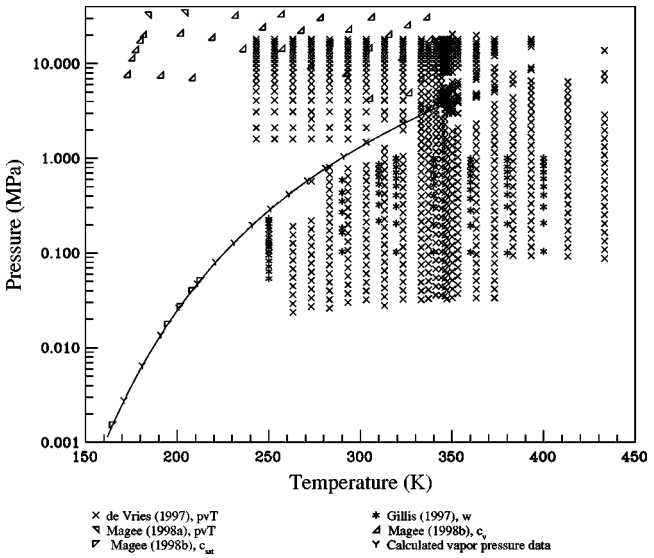

FIG. 12. Selected data used in determining the coefficients of the equation of state.

in density. Excluding the critical region from 347 to 354 K and 2 to 7 mol/dm^3, the average absolute deviation for these data decreases to 0.03% for all data. The average deviations (excluding the critical region) are 0.06% for the data of Weber and Defibaugh (1996), 0.08% for the data of Zhang *et al.* (1995), and 0.18% for the data of Nakamura *et al.* (1997). In the extended critical region from 340 to 390 K and 3 to 9 mol/dm^3 (as shown in Fig. 14), average absolute deviations in pressure between experimental data and the equation of state are 0.14% for the data of de Vries, 0.23% for the data of Nakamura *et al.* (1997), and 0.11% for the data of Tsuge *et al.* (1997).

Table 7 summarizes the sources for the second virial coefficients of R-143a. Additional values for the second virial coefficient were numerically determined by fitting $(Z-1)/\rho$ as a function of density using the data of de Vries (1997). The additional data are shown in Fig. 15 as circles. These values are given in Table 8. Data below 0.1 mol/dm^3 were not used since such low density data may be subject to local adsorption by the walls of the apparatus or to higher uncertainties in the measurement of extremely low pressures. The solid lines show isotherms calculated from the equation of state presented here and the solid curve represents the saturated vapor density. The *y* intercept (zero density) represents the second virial coefficient at a given temperature, and the third virial coefficient can be taken from the slope of each line at zero density. The values of the second virial coefficient calculated from the equation of state (the values of the lines in the figure at zero density) agree well with those determined numerically and shown as circles in the figure. Comparisons of second virial coefficients calculated with the equation of state and those determined here (given in Table 8) are shown in Fig. 16. For the lowest two isotherms (263 and 273 K), the uncertainty in the calculated values is higher due to the limited data at densities above 0.1 mol/dm^3 and to the higher curvature in the data. Figure

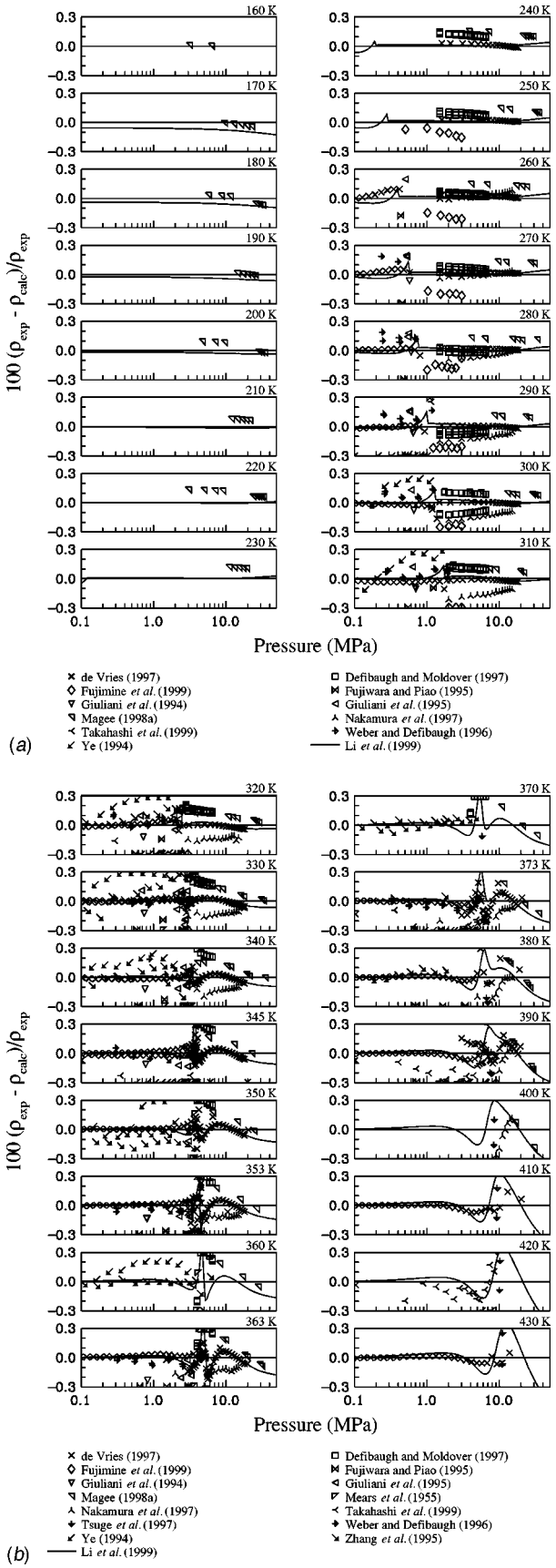

FIG. 13. Comparisons of densities calculated with the equation of state to experimental data.

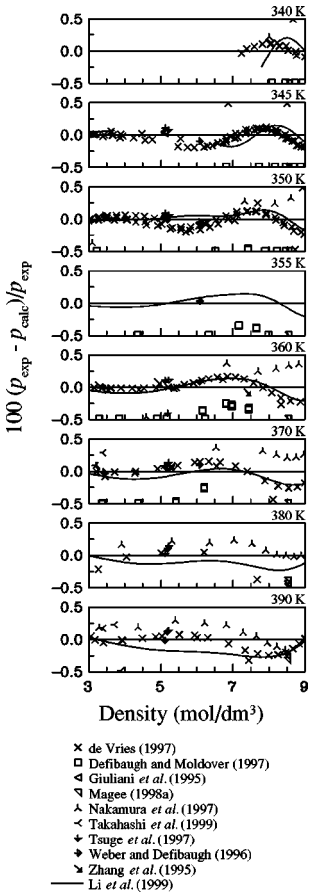

FIG. 14. Comparisons of pressures calculated with the equation of state to experimental data in the critical region.

16 shows comparisons with other reported second virial coefficients as well, showing good agreement between the equation of state and the values reported by Zhang *et al.* (1995), Beckermann and Kohler (1995), and Gillis (1997).

4.3. Caloric Data

The sources of experimental data for the speed of sound of R-143a are summarized in Table 9 and shown graphically in

TABLE 7. Summary of second virial coefficients

Author	No. of points	Temp. range (K)	AAD[a] (cm^3/mol)
Beckermann and Kohler (1995)	9	250–410	3.7
Bignell and Dunlop (1993)	3	290–310	4.3
de Vries (1997)[b]	21	263–433	1.1
Gillis (1997)	7	250–400	3.4
Ye (1994)	7	300–360	12.
Zhang *et al.* (1995)	7	320–380	0.74
Overall	54	250–433	3.4

[a]Average absolute difference in the second virial coefficient (cm^3/mol).
[b]Data were derived from the $p\rho T$ data of de Vries and are given in Table 8. The data were used in the development of the equation of state.

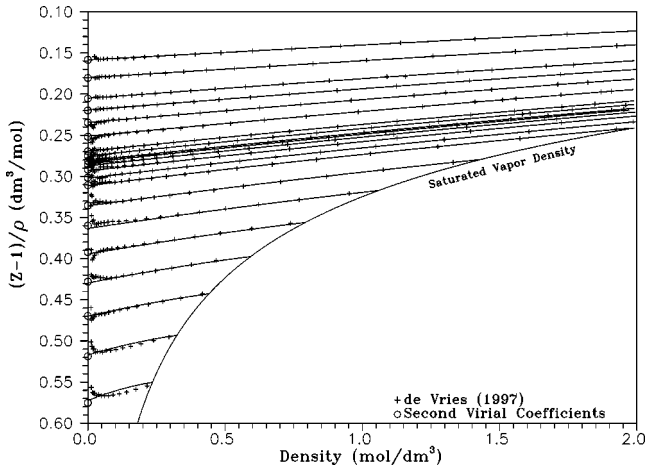

FIG. 15. Derivation of second virial coefficients from the $p\rho T$ data of de Vries (1997).

TABLE 8. Second virial coefficients derived from the $p\rho T$ data of de Vries (1997)

Temp. (K)	B (dm^3/mol)	Temp. (K)	B (dm^3/mol)
263.15	−0.5752	346.15	−0.2811
273.15	−0.5187	347.15	−0.2813
283.15	−0.4696	350.15	−0.2749
293.15	−0.4280	353.15	−0.2694
303.15	−0.3920	363.15	−0.2518
313.15	−0.3598	373.15	−0.2347
323.15	−0.3353	383.15	−0.2199
333.15	−0.3107	393.15	−0.2054
337.15	−0.3015	413.15	−0.1804
341.15	−0.2918	433.15	−0.1584
344.15	−0.2855		

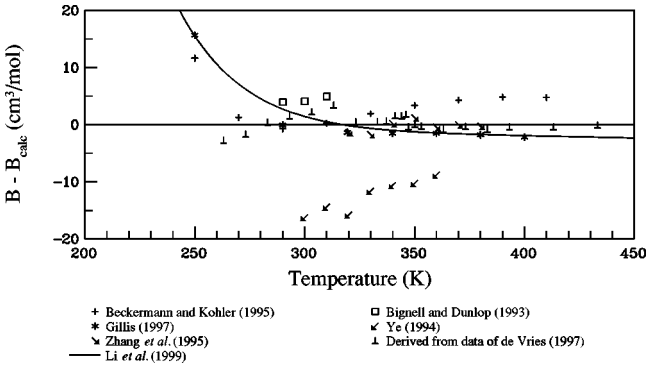

FIG. 16. Comparisons of second virial coefficients calculated with the equation of state to experimental data.

TABLE 9. Summary of speed of sound data

Author	No. of points	Temp. range (K)	Pressure range (MPa)	AAD (%)
Vapor phase data				
Beckermann and Kohler (1997)	246	250–410	0.02–0.5	0.024
Gillis (1997)[a]	86	250–400	0.05–1.0	0.013
Ogawa and Sato (1999)	70	303–343	0.01–0.5	0.003
Overall	402	250–410	0.01–1.0	0.018
Liquid phase and saturation data				
Froeba *et al.* (2000)	16	288–345	sat. liq.	1.03
Froeba *et al.* (2000)	12	313–346	sat. vap.	0.68
Takagi (1997)	189	243–333	0.21–30.	0.27
Overall	217	243–346	0.21–30.	0.35

[a]Data used in the development of the equation of state.

Fig. 17. Comparisons of values calculated from the equation of state for the speed of sound are shown in Fig. 18 for the vapor phase and in Fig. 19 for the liquid phase. The equation represents the vapor phase data of Beckermann and Kohler (1997), Gillis (1997), and Ogawa and Sato (1999) within 0.02% and the liquid phase data of Takagi (1997) within 0.5%. There are no speed of sound data below 240 K, however, the extrapolation behavior shown in Sec. 4.4 is quite reasonable at low temperatures.

The reported measurements of the isochoric heat capacity, saturated liquid heat capacity, and isobaric heat capacity for R-143a are summarized in Table 10 and also illustrated in Fig. 17. Comparisons of values calculated from the equation of state are shown for the isochoric heat capacities in Fig. 20, saturated liquid heat capacities in Fig. 21, and isobaric heat capacities in Fig. 22. Magee (1998b) measured both the isochoric heat capacity of R-143a and the heat capacity along the saturated liquid line. The average deviation between

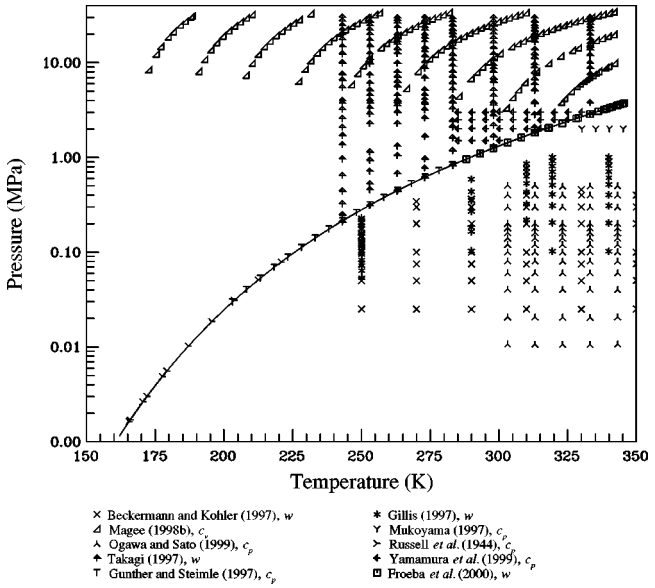

FIG. 17. Isobaric and isochoric heat capacities and speed of sound data.

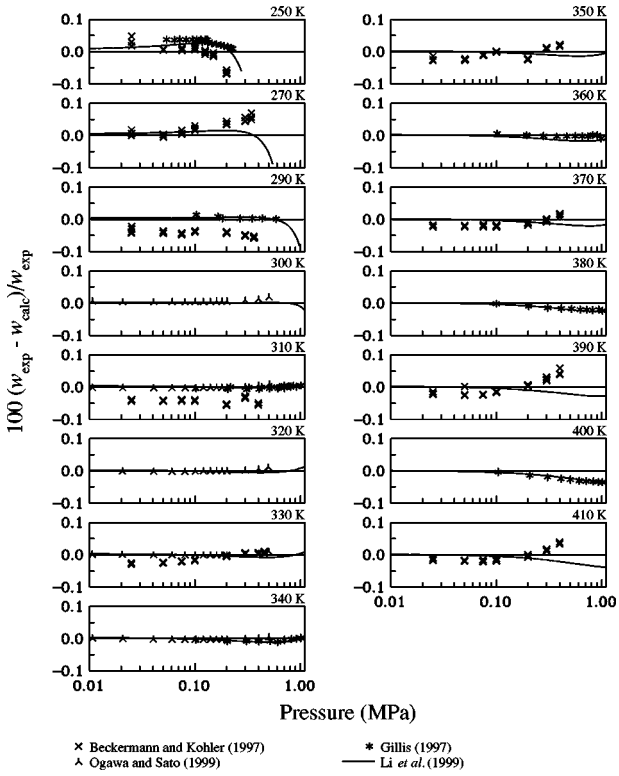

FIG. 18. Comparisons of speeds of sound in the vapor phase calculated with the equation of state to experimental data.

these data and the equation of state is 0.25% for the isochoric heat capacity and 0.47% for the saturated liquid heat capacity. The deviations of the latter set increase as the temperature approaches the critical temperature (i.e., the average deviation is 0.24% rather than 0.47% if the two highest points are discarded), however, the uncertainties in these higher temperature data points also increase as discussed by Magee. The sparse information concerning the isobaric heat capacity of R-143a includes four points in the vapor phase by

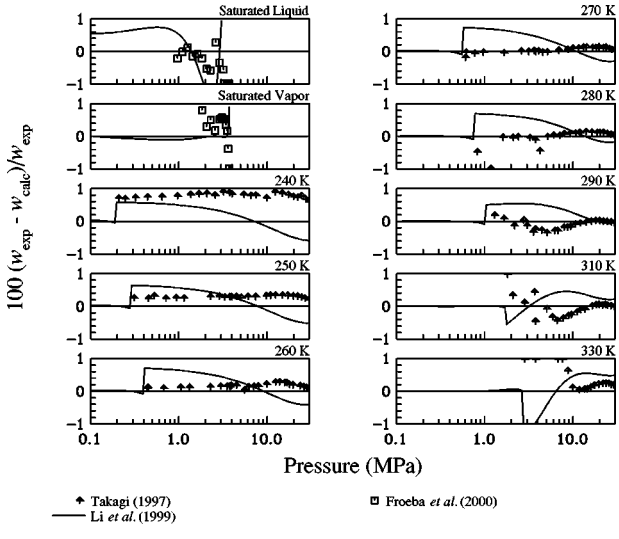

FIG. 19. Comparisons of speeds of sound in the liquid phase calculated with the equation of state to experimental data.

TABLE 10. Summary of experimental heat capacity data

Author	No. of points	Temp. range (K)	Density range (mol/dm^3)	Pressure range (MPa)	AAD (%)
Isochoric heat capacity data					
Magee (1998b)[a]	136	173–342	10.–16.		0.25
Saturated heat capacity data					
Magee (1998b)[a]	80	165–343			0.47
Isobaric heat capacity data					
Gunther and Steimle (1997)	24	203–318		sat. liq.	0.69
Mukoyama (1997) (1996)	4	330–345		2.0	0.42
Russell *et al.* (1944)	11	165–221		sat. liq.	0.16
Yamamura *et al.* (1999)	30	285–330		1.5–3.0	0.51
Overall	69	165–345		1.5–3.0	0.51

[a]Data used in the development of the equation of state.

Mukoyama *et al.* (1997), 30 points in the liquid phase by Yamamura *et al.* (1999), 11 points along the saturated liquid line at low temperatures by Russell *et al.* (1944), and 24 points along the saturated liquid line by Gunther and Steimle (1997). Although none of these data were used in the fit, the equation of state represents the data of Russell *et al.* within 0.16%. This good agreement indicates consistency between the fitted isochoric and saturated heat capacity data of Magee and the isobaric heat capacity data of Russell. Average differences between the experimental data of Yamamura *et al.* and calculated values from the equation of state are 0.5%. Differences are as high as 1.5% in the region of overlap between the data of Russel *et al.* and Gunther and Steimle. Additional experimental information on the isobaric heat capacity in the liquid is needed to help resolve the differences between the various data sets.

4.4. Extrapolation Behavior

Plots of certain characteristic curves are useful in assessing the behavior of an equation of state in regions away from the available data (Deiters and de Reuck, 1997, Span and Wagner, 1997, Span, 2000). The characteristic curves considered in this work are the Boyle curve, given by the equation

$$\left(\frac{\partial Z}{\partial v}\right)_T = 0, \tag{44}$$

the Joule–Thomson inversion curve

$$\left(\frac{\partial Z}{\partial T}\right)_p = 0, \tag{45}$$

the Joule inversion curve

$$\left(\frac{\partial Z}{\partial T}\right)_v = 0, \tag{46}$$

and the ideal curve

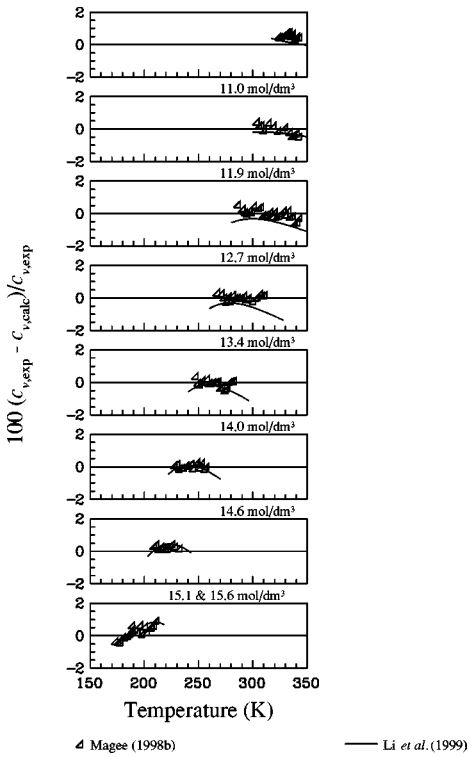

FIG. 20. Comparisons of isochoric heat capacities calculated with the equation of state to experimental data.

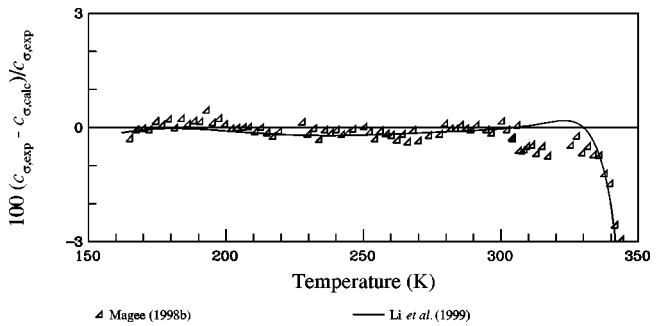

FIG. 21. Comparisons of saturated heat capacities calculated with the equation of state to experimental data.

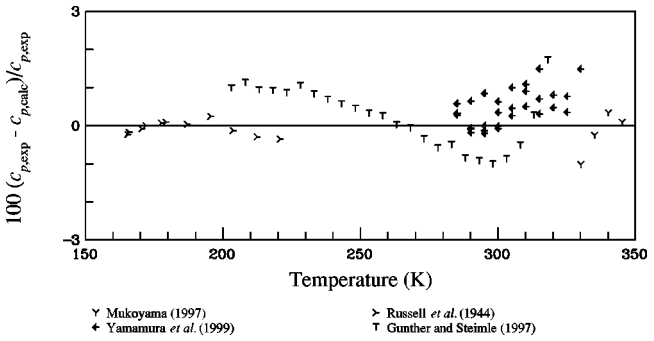

FIG. 22. Comparisons of isobaric heat capacities calculated with the equation of state to experimental data.

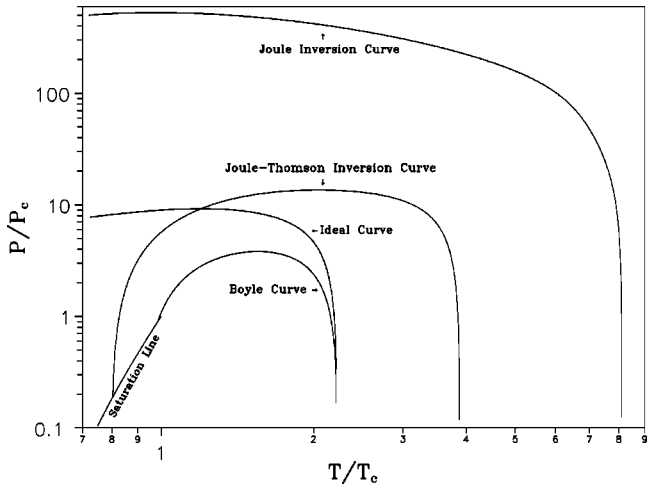

FIG. 23. Characteristic curves.

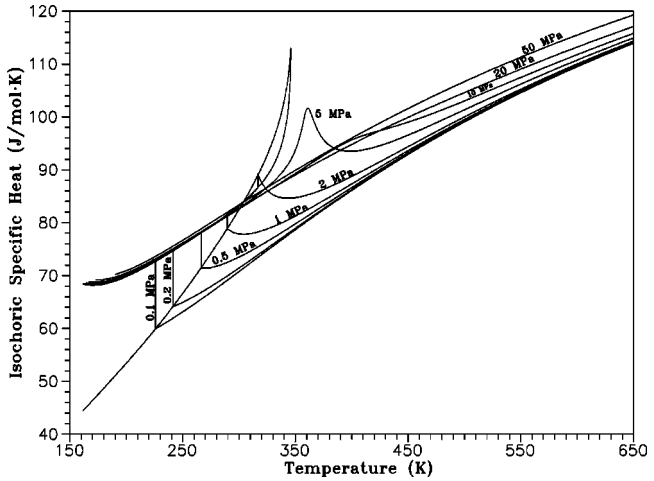

FIG. 24. Isochoric heat capacity versus temperature diagram.

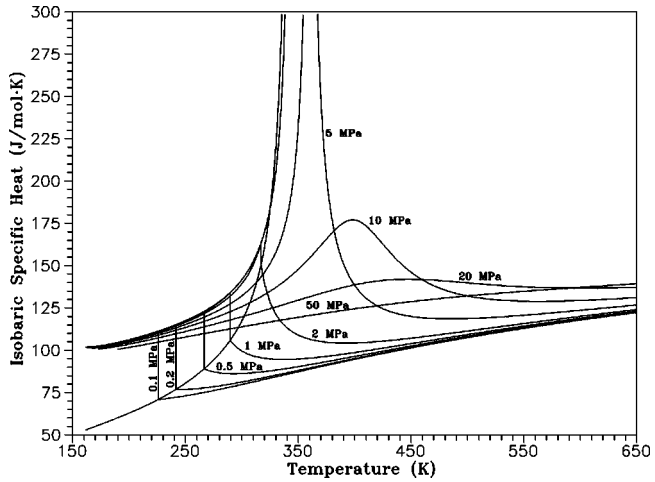

FIG. 25. Isobaric heat capacity versus temperature diagram.

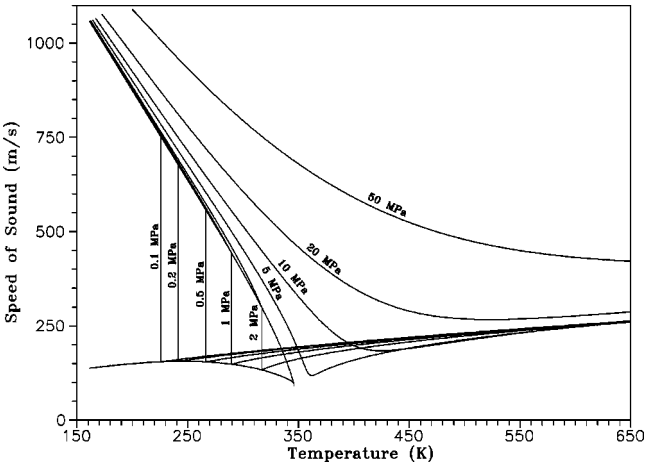

FIG. 26. Speed of sound versus temperature diagram.

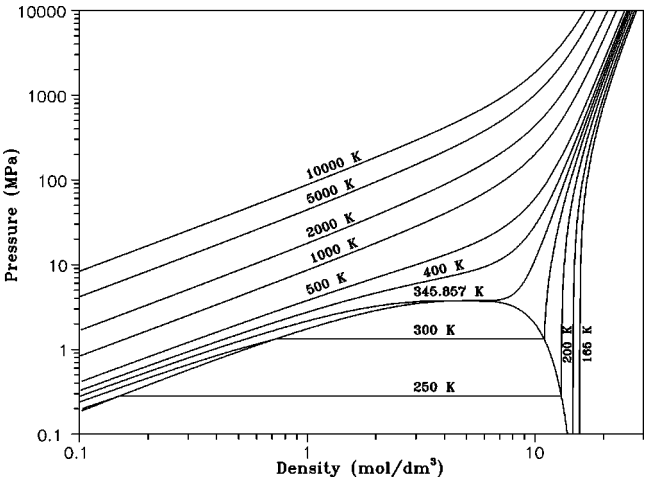

FIG. 27. Pressure versus density diagram.

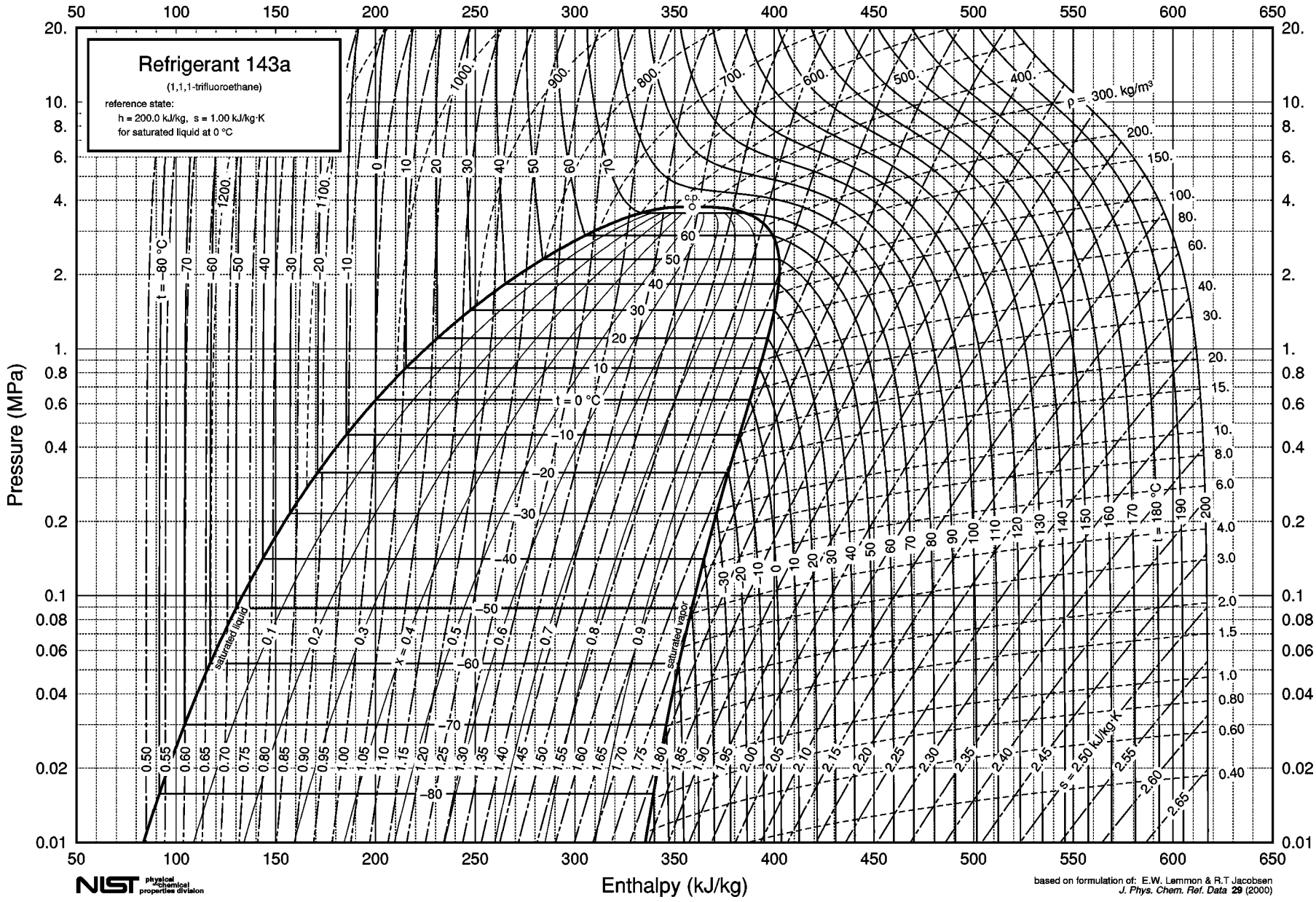

FIG. 28. Pressure versus enthalpy diagram.

$$\frac{p}{\rho RT} = 1. \tag{47}$$

These characteristic curves for the equation of state for R-143a are illustrated in Fig. 23. Although the curves in this figure do not provide numerical information, the reasonable shapes of these curves as shown indicate qualitatively correct extrapolation behavior of the equation of state extending to extremely high pressures and temperatures far in excess of the likely thermal stability of the fluid.

Plots of constant property lines on various thermodynamic coordinates are useful in assessing the behavior of the equation of state. The equation developed here was used to produce plots of temperature versus isochoric heat capacity (Fig. 24), isobaric heat capacity (Fig. 25), and speed of sound (Fig. 26). These plots indicate that the equation of state exhibits reasonable behavior over all temperatures and pressures within the range of validity and that the extrapolation behavior is reasonable at higher temperatures and pressures. Figure 27 verifies that the equation of state extrapolates to extremely high temperatures and pressures, however, much of this diagram is well above the region where R143a dissociates, and these regions are shown only to illustrate the well behaved nature of the equation.

5. Estimated Uncertainty of Calculated Properties

The new reference equation of state describes the $p\rho T$ surface with an uncertainty of 0.1% in density at temperatures from the triple point to 450 K and pressures up to 50 MPa. In the gaseous and supercritical region, speed of sound data are represented within 0.02% at pressures below 1 MPa. The estimated uncertainty for heat capacities is 0.5% and the estimated uncertainty for the speed of sound in the liquid phase is 0.5% for $T > 250$ K. The saturation values can be calculated from the equation of state by application of the Maxwell criterion, which requires equal Gibbs energies and equal pressures for saturated liquid and vapor states at the same temperature. The estimated uncertainties of vapor pressures and saturated liquid densities calculated using the Maxwell criterion are 0.1% for each property, except in the critical region, and the estimated uncertainty for saturated vapor density is 0.2%. Based on graphical verification of the derived properties, the equation can be extended to 650 K with estimated uncertainties of 0.2% in density and 1.0% in heat capacities and sound speeds.

6. Acknowledgments

We gratefully acknowledge the suggestions of Mark McLinden, Reiner Tillner-Roth, Koichi Watanabe, Yukihiro Higashi, Haruki Sato, and Chun-Cheng Piao, all of whom were participants of the IEA Annex-18 projects and contributed to the discussion and development of the many equations of state resulting from that work. Their friendship and cooperation have resulted in international standards that would not have been possible otherwise. We are also grateful for the many discussions with Joe Magee and Roland Span concerning the data and new fitting procedures that were used during this work. We dedicate this work to Dr. Lloyd Weber, a colleague and friend who passed away on August 15, 1999, whose careful experimental procedures provided some of the key data used in this work.

7. References

Aoyama, H., G. Kishizawa, H. Sato, and K. Watanabe, J. Chem. Eng. Data **41**, 1046 (1996).
Arnaud, D., S. Macaudiere, L. Niveau, and S. Wosinski, Proc. 18th Int. Congr. Refrig. **2**, 664 (1991).
Beckermann, W. and F. Kohler, Int. J. Thermophys. **16**, 455 (1995).
Beckermann, W. and F. Kohler (private communication, 1997).
Bignell, C. M. and P. J. Dunlop, J. Chem. Phys. **98**, 4889 (1993).
Chen, S. S., A. S. Rodgers, J. Chao, R. C. Wilhoit, and B. J. Zwolinski, J. Phys. Chem. Ref. Data **4**, 441 (1975).
Defibaugh, D. R. and M. R. Moldover, J. Chem. Eng. Data **42**, 160 (1997).
Deiters, U. K. and K. M. de Reuck, Pure Appl. Chem. **69**, 1237 (1997).
de Vries, B., Dissertation, University of Hannover, Germany, 1997.
Doering, R., H. Buchwald, and C. von Eynatten, Oesterreichischer Kaelte- und Klimatechnischer Verein (1994).
Duarte-Garza, H. A. and J. W. Magee, Int. J. Thermophys. **20**, 1467 (1999).
Froeba, A. P., S. Will, and A. Leipertz, Int. J. Thermophys. (submitted, 2000).
Fujimine, T., H. Sato, and K. Watanabe, Int. J. Thermophys. **20**, 911 (1999).
Fujiwara, K. and C.-C. Piao, Prop. 16th Japan Symp. Thermophys. Prop., Hiroshima, 1995, p. 161.
Fujiwara, K., S. Nakamura, and M. Noguchi, J. Chem. Eng. Data **43**, 55 (1998).
Fukushima, M., Trans. Jpn. Assoc. Ref. **10**, 87 (1993).
Gillis, K. A., Int. J. Thermophys. **18**, 73 (1997).
Giuliani, G., S. Kumar, F. Polanara, and P. Zazzini, Proc. of the Int. Conf. ''CFCs, The day after,'' Joint Meeting of IIR Commissions B1, B2, E1 and E2, Padova, Italy, 1994.
Giuliani, G., S. Kumar, P. Zazzini, and F. Polanara, J. Chem. Eng. Data **40**, 903 (1995).
Gunther, D. and F. Steimle, Int. J. Refrig. **20**, 235 (1997).
Higashi, Y. and T. Ikeda, Fluid Phase Equilib. **125**, 139 (1996).
Kilner, J. and R. J. B. Craven, IEA Heat Pump Programme Report No. HPP-AN18-4, Sittard, The Netherlands (1997).
Kubota, H., N. Nojiri, and T. Makita, Rev. Phys. Chem. Jpn. Sp. Vol., p. 1 (1990).
Lemmon, E. W., Evaluation of Thermodynamic Property Models for Mixtures of R-32, R-125, and R-134a, IEA Heat Pump Centre, Sittard, The Netherlands (1998).
Lemmon, E. W., R. T Jacobsen, S. G. Penoncello, and D. G. Friend, J. Phys. Chem. Ref. Data **29**, 331 (2000).
Li, J., R. Tillner-Roth, H. Sato, and K. Watanabe, Int. J. Thermophys. **20**, 1639 (1999).
Magee, J. W., Int. J. Thermophys. **19**, 1381 (1998a).
Magee, J. W., Int. J. Thermophys. **19**, 1397 (1998b).
Mears, W. H., R. F. Stahl, S. R. Orfeo, R. C. Shair, L. F. Kells, W. Thompson, and H. McCann, Ind. Eng. Chem. **47**, 1449 (1955).
Mohr, P. J. and B. N. Taylor, J. Phys. Chem. Ref. Data **28**, 1713 (1999).
Mukoyama, K., Masters Thesis, Keio University, Yokohama, Japan, 1996. Also described in: Mukoyama, K., Sato, H., Watanabe, K., International Conference on High Pressure Science and Technology, Kyoto, Japan, 1997, p. 158.
Nagel, M. and K. Bier, Int. J. Refrig. **19**, 264 (1996).
Nakamura, S., K. Fujiwara, and M. Noguchi, J. Chem. Eng. Data **42**, 334 (1997).
Ogawa, K. and H. Sato, Int. J. Thermophys (submitted, 1999).
Outcalt, S. L. and M. O. McLinden, Int. J. Thermophys. **18**, 1445 (1997).
Penoncello, S. G., R. T Jacobsen, M. de Reuck, A. E. Elhassan, R. C. Williams, and E. W. Lemmon, Int. J. Thermophys. **16**, 781 (1995).

Piao, C.-C. and M. Noguchi, J. Phys. Chem. Ref. Data **27**, 775 (1998).
Piao, C.-C., K. Fujiwara, and M. Noguchi, Fluid Phase Equilib. **151**, 303 (1998).
Preston-Thomas, H., Metrologia **27**, 3 (1990).
Russell, H. D. R., V. Golding, and D. M. Yost, J. Am. Chem. Soc. **66**, 16 (1944).
Schmidt, J. W., E. Carrillo-Nava, and M. R. Moldover, Fluid Phase Equilib. **122**, 187 (1996).
Smith, D. C., G. M. Brown, J. R. Nielsen, R. M. Smith, and C. Y. Liang, J. Chem. Phys. **20**, 473 (1952).
Span, R., *Multiparameter Equations of State-An Accurate Source of Thermodynamic Property Data* (Springer, Berlin, 2000).
Span, R. and W. Wagner, Int. J. Thermophys. **18**, 1415 (1997).
Sunaga, H., R. Tillner-Roth, H. Sato, and K. Watanabe, Int. J. Thermophys. **19**, 1623 (1998).
Takagi, T., J. Chem. Eng. Data **42**, 1129 (1997).
Takahashi, M., N. Shibasaki-Kitakawa, and C. Yokoyama, Int. J. Thermophys. **20**, 435 (1999).
Takashima, H. and Y. Higashi, Proc. 16th Japan Symp. Thermophys. Prop., Hiroshima, Japan, 1995, p. 9.
Tillner-Roth, R. and H. D. Baehr, J. Phys. Chem. Ref. Data **23**, 657 (1994).
Tillner-Roth, R. and A. Yokozeki, J. Phys. Chem. Ref. Data **25**, 1273 (1997).
Tsuge, T., H. Sato, and K. Watanabe, Keio University (private communication, 1997).
Vanderkooi, W. N. and T. de Vries, J. Phys. Chem. **60**, 636 (1956).
Wagner, W., Fortschr.-Ber. VDI, Dusseldorf, VDI-Verlag **3**, (1974).
Wang, H., Y. Ma, C. Lu, and Y. Tian, Beijing Gongcheng Rewuli Xuebao **14**, 122 (1993).
Weber, L. A. and D. R. Defibaugh, J. Chem. Eng. Data **41**, 1477 (1996).
Widiatmo, J. V., H. Sato, and K. Watanabe, J. Chem. Eng. Data **39**, 304 (1994).
Yamamura, T., G. Yasuda, H. Sato, and K. Watanabe, J. Chem. Eng. Data (submitted, 1999).
Ye, F., Masters Thesis, Keio University, Yokohama, Japan, 1994.
Yokoyama, C. and S. Takahashi, Fluid Phase Equilib. **67**, 227 (1991).
Yokozeki, A., H. Sato, and K. Watanabe, Int. J. Thermophys. **19**, 89 (1998).
Younglove, B. A. and M. O. McLinden, J. Phys. Chem. Ref. Data **23**, 731 (1994).
Zhang, H.-L., H. Sato, and K. Watanabe, J. Chem. Eng. Data **40**, 887 (1995).

8. Appendix—Tables of Thermodynamic Properties of R-143a

Thermodynamic Properties of R-143a at Saturation

t (°C)	p (MPa)	ρ (kg/m^3)	h (kJ/kg)	s (kJ/(kg K))	c_v (kJ/(kg K))	c_p (kJ/(kg K))	w (m/s)
−111.810	0.001 07	1330.5	52.520	.314 17	0.8138	1.211	1058.1
		0.067 54	319.59	1.9695	0.5283	0.6299	137.6
−110.	0.001 29	1326.2	54.713	.327 69	0.8128	1.212	1049.4
		0.080 45	320.68	1.9579	0.5331	0.6350	138.2
−105.	0.002 11	1314.1	60.780	.364 31	0.8114	1.215	1025.5
		0.127 45	323.73	1.9281	0.5467	0.6495	140.0
−100.	0.003 33	1301.9	66.868	.399 98	0.8115	1.220	1001.7
		0.195 59	326.81	1.9012	0.5604	0.6642	141.7
−95.	0.005 10	1289.6	72.983	.434 79	0.8131	1.226	977.9
		0.291 68	329.92	1.8770	0.5742	0.6792	143.3
−90.	0.007 61	1277.2	79.132	.468 82	0.8157	1.233	954.2
		0.423 80	333.06	1.8553	0.5881	0.6944	144.9
−85.	0.011 06	1264.8	85.320	.502 14	0.8194	1.241	930.4
		0.601 41	336.22	1.8357	0.6021	0.7100	146.4
−80.	0.015 72	1252.2	91.552	.534 81	0.8238	1.250	906.6
		0.835 35	339.40	1.8180	0.6162	0.7258	147.8
−75.	0.021 89	1239.5	97.831	.566 88	0.8288	1.260	882.8
		1.1379	342.60	1.8021	0.6304	0.7421	149.1
−70.	0.029 91	1226.7	104.16	.598 39	0.8344	1.270	859.1
		1.5227	345.80	1.7879	0.6448	0.7589	150.4
−65.	0.040 16	1213.7	110.54	.629 39	0.8405	1.281	835.3
		2.0048	349.01	1.7750	0.6593	0.7763	151.5
−60.	0.053 07	1200.6	116.99	.659 92	0.8470	1.293	811.5
		2.6011	352.21	1.7635	0.6741	0.7944	152.5
−55.	0.069 09	1187.3	123.49	.690 00	0.8538	1.305	787.7
		3.3295	355.41	1.7531	0.6892	0.8133	153.4
−50.	0.088 74	1173.9	130.05	.719 68	0.8608	1.318	763.9
		4.2098	358.58	1.7438	0.7046	0.8331	154.2
−45.	0.112 55	1160.3	136.68	.748 97	0.8681	1.331	740.1
		5.2637	361.74	1.7354	0.7203	0.8539	154.8
−40.	0.141 09	1146.4	143.38	.777 91	0.8756	1.345	716.3
		6.5145	364.86	1.7279	0.7363	0.8758	155.3
−35.	0.174 99	1132.3	150.15	.806 53	0.8833	1.360	692.5
		7.9877	367.95	1.7211	0.7526	0.8989	155.7
−30.	0.214 88	1117.9	157.00	.834 85	0.8911	1.375	668.6
		9.7113	370.99	1.7149	0.7693	0.9233	155.8
−25.	0.261 44	1103.3	163.93	.862 89	0.8991	1.392	644.7
		11.716	373.98	1.7093	0.7863	0.9492	155.8
−20.	0.315 35	1088.3	170.95	.890 69	0.9072	1.409	620.8
		14.036	376.91	1.7043	0.8035	0.9767	155.7
−15.	0.377 37	1072.9	178.06	.918 27	0.9154	1.428	596.8
		16.709	379.76	1.6996	0.8211	1.006	155.3
−10.	0.448 23	1057.2	185.27	.945 67	0.9237	1.449	572.8
		19.778	382.54	1.6953	0.8390	1.038	154.8
−5.	0.528 73	1041.0	192.58	.972 90	0.9322	1.471	548.6
		23.292	385.23	1.6913	0.8571	1.072	154.0
0.	0.619 67	1024.3	200.00	1.0000	0.9408	1.495	524.3
		27.306	387.81	1.6876	0.8756	1.109	153.1
5.	0.721 90	1007.0	207.54	1.0270	0.9495	1.522	499.8
		31.885	390.27	1.6839	0.8944	1.149	151.9
10.	0.836 28	989.06	215.22	1.0539	0.9585	1.552	475.1
		37.107	392.60	1.6804	0.9135	1.194	150.4
15.	0.963 72	970.37	223.04	1.0809	0.9678	1.585	450.2
		43.062	394.77	1.6768	0.9331	1.245	148.7
20.	1.105 15	950.80	231.03	1.1078	0.9773	1.624	425.0
		49.864	396.76	1.6732	0.9531	1.302	146.8
25.	1.261 57	930.22	239.19	1.1349	0.9873	1.669	399.5
		57.653	398.54	1.6693	0.9737	1.369	144.5
30.	1.434 00	908.45	247.56	1.1621	0.9978	1.722	373.5

Thermodynamic Properties of R-143a at Saturation—Continued

t (°C)	p (MPa)	ρ (kg/m^3)	h (kJ/kg)	s (kJ/(kg K))	c_v (kJ/(kg K))	c_p (kJ/(kg K))	w (m/s)
		66.605	400.07	1.6652	0.9951	1.449	141.9
35.	1.623 55	885.23	256.16	1.1895	1.009	1.786	347.0
		76.954	401.31	1.6606	1.017	1.547	139.0
40.	1.831 41	860.25	265.04	1.2174	1.021	1.867	319.8
		89.018	402.19	1.6553	1.041	1.671	135.7
45.	2.058 86	833.06	274.26	1.2457	1.035	1.972	291.8
		103.24	402.61	1.6491	1.066	1.837	132.0
50.	2.307 35	802.97	283.90	1.2748	1.051	2.118	262.7
		120.31	402.43	1.6416	1.093	2.070	127.9
55.	2.578 53	768.90	294.09	1.3051	1.070	2.337	232.2
		141.30	401.44	1.6322	1.124	2.430	123.2
60.	2.874 42	728.86	305.09	1.3371	1.095	2.714	199.5
		168.24	399.24	1.6197	1.159	3.069	117.9
65.	3.197 70	678.34	317.45	1.3726	1.131	3.564	163.8
		205.65	394.94	1.6018	1.204	4.532	111.8
70.	3.552 68	600.85	333.19	1.4172	1.198	7.720	122.4
		270.10	385.42	1.5694	1.272	11.50	104.2
72.707	3.761 00	431.00	358.91	1.4906			

t (°C)	p (MPa)	ρ (kg/m^3)	h (kJ/kg)	s (kJ/(kg K))	c_v (kJ/(kg K))	c_p (kJ/(kg K))	w (m/s)
−111.810	0.001 07	1330.5	52.520	.314 17	0.8138	1.211	1058.1
		0.067 54	319.59	1.9695	0.5283	0.6299	137.6
−76.395	0.02	1243.0	96.074	.557 98	0.8274	1.257	889.5
		1.0458	341.71	1.8064	0.6264	0.7375	148.8
−65.070	0.04	1213.9	110.45	.628 96	0.8404	1.281	835.6
		1.9973	348.96	1.7752	0.6591	0.7760	151.5
−57.706	0.06	1194.5	119.96	.673 77	0.8501	1.298	800.6
		2.9177	353.68	1.7586	0.6810	0.8029	152.9
−52.102	0.08	1179.6	127.28	.707 25	0.8578	1.312	773.9
		3.8198	357.25	1.7476	0.6981	0.8246	153.9
−47.518	0.10	1167.1	133.33	.734 26	0.8644	1.324	752.1
		4.7099	360.15	1.7395	0.7123	0.8433	154.5
−47.241	0.101 325	1166.4	133.70	.735 89	0.8648	1.325	750.8
		4.7685	360.33	1.7391	0.7132	0.8444	154.6
−38.603	0.15	1142.5	145.27	.785 94	0.8778	1.349	709.6
		6.9025	365.73	1.7259	0.7408	0.8821	155.4
−31.774	0.20	1123.1	154.56	.824 83	0.8883	1.370	677.1
		9.0691	369.92	1.7170	0.7633	0.9145	155.8
−26.161	0.25	1106.7	162.32	.856 40	0.8972	1.388	650.3
		11.224	373.29	1.7106	0.7823	0.9430	155.9
−21.353	0.30	1092.4	169.05	.883 19	0.9050	1.405	627.3
		13.375	376.12	1.7056	0.7988	0.9691	155.7
−17.123	0.35	1079.5	175.03	.906 59	0.9119	1.420	607.0
		15.528	378.56	1.7015	0.8136	0.9934	155.5
−13.331	0.40	1067.7	180.46	.927 44	0.9181	1.435	588.8
		17.687	380.70	1.6981	0.8270	1.016	155.2
−9.883	0.45	1056.8	185.44	.946 30	0.9239	1.449	572.2
		19.855	382.60	1.6952	0.8394	1.038	154.8
−6.714	0.50	1046.6	190.06	.963 58	0.9292	1.463	556.9
		22.034	384.32	1.6927	0.8509	1.060	154.3
−3.776	0.55	1037.0	194.38	.979 54	0.9342	1.477	542.6
		24.226	385.87	1.6904	0.8616	1.080	153.8
−1.032	0.60	1027.8	198.46	.994 41	0.9390	1.490	529.3
		26.433	387.28	1.6883	0.8718	1.101	153.3
1.544	0.65	1019.0	202.32	1.0083	0.9435	1.503	516.7
		28.656	388.58	1.6864	0.8814	1.121	152.7
3.976	0.70	1010.6	205.99	1.0215	0.9477	1.516	504.8
		30.898	389.77	1.6847	0.8905	1.141	152.1
6.281	0.75	1002.5	209.50	1.0339	0.9518	1.529	493.5
		33.158	390.88	1.6830	0.8992	1.160	151.5
8.473	0.80	994.62	212.86	1.0457	0.9558	1.542	482.7
		35.439	391.90	1.6815	0.9076	1.180	150.9

Thermodynamic Properties of R-143a at Saturation—Continued

t (°C)	p (MPa)	ρ (kg/m^3)	h (kJ/kg)	s (kJ/(kg K))	c_v (kJ/(kg K))	c_p (kJ/(kg K))	w (m/s)
10.565	0.85	986.99	216.10	1.0570	0.9596	1.555	472.3
		37.741	392.85	1.6800	0.9157	1.200	150.3
12.566	0.90	979.57	219.22	1.0678	0.9632	1.568	462.4
		40.065	393.73	1.6786	0.9235	1.219	149.6
14.486	0.95	972.32	222.23	1.0781	0.9668	1.582	452.8
		42.414	394.55	1.6772	0.9310	1.239	148.9
16.332	1.00	965.24	225.15	1.0880	0.9703	1.595	443.5
		44.787	395.32	1.6759	0.9384	1.259	148.2
19.827	1.10	951.50	230.75	1.1069	0.9770	1.622	425.9
		49.613	396.69	1.6733	0.9524	1.300	146.8
23.091	1.20	938.21	236.05	1.1245	0.9834	1.651	409.3
		54.552	397.89	1.6708	0.9658	1.343	145.4
26.157	1.30	925.30	241.11	1.1412	0.9897	1.680	393.5
		59.613	398.92	1.6684	0.9786	1.387	143.9
29.051	1.40	912.68	245.95	1.1569	0.9958	1.711	378.5
		64.807	399.80	1.6660	0.9910	1.433	142.4
31.794	1.50	900.29	250.61	1.1719	1.002	1.743	364.1
		70.144	400.56	1.6636	1.003	1.482	140.9
34.403	1.60	888.09	255.12	1.1863	1.008	1.778	350.2
		75.637	401.18	1.6612	1.015	1.534	139.4
36.892	1.70	876.01	259.49	1.2000	1.014	1.815	336.8
		81.298	401.69	1.6587	1.026	1.591	137.8
39.273	1.80	864.01	263.73	1.2133	1.019	1.854	323.8
		87.142	402.09	1.6561	1.037	1.651	136.2
43.748	2.00	840.11	271.92	1.2386	1.031	1.943	298.9
		99.448	402.55	1.6508	1.059	1.790	133.0
47.894	2.20	816.06	279.78	1.2625	1.044	2.050	275.2
		112.72	402.59	1.6450	1.081	1.961	129.7
51.758	2.40	791.52	287.41	1.2853	1.057	2.184	252.2
		127.16	402.19	1.6386	1.103	2.178	126.3
55.378	2.60	766.12	294.89	1.3074	1.072	2.358	229.8
		143.09	401.33	1.6314	1.126	2.466	122.8
58.783	2.80	739.32	302.32	1.3291	1.088	2.599	207.7
		160.96	399.92	1.6232	1.150	2.871	119.3
61.996	3.00	710.37	309.81	1.3507	1.108	2.959	185.7
		181.48	397.86	1.6135	1.176	3.489	115.6
65.034	3.20	677.94	317.54	1.3728	1.132	3.573	163.5
		205.96	394.90	1.6016	1.205	4.549	111.8
67.910	3.40	639.25	325.86	1.3964	1.163	4.887	140.6
		237.14	390.54	1.5861	1.239	6.801	107.7
70.629	3.60	585.69	335.85	1.4247	1.213	9.788	116.5
		283.61	383.21	1.5624	1.284	14.81	103.0
72.707	3.761	431.00	358.91	1.4906			

Thermodynamic Properties of R-143a

t (°C)	ρ (kg/m^3)	u (kJ/kg)	h (kJ/kg)	s (kJ/(kg K))	c_v (kJ/(kg K))	c_p (kJ/(kg K))	w (m/s)
			0.1 MPa				
−100.	1302.0	66.841	66.918	.399 84	0.8116	1.220	1002.1
−90.	1277.4	79.100	79.179	.468 68	0.8158	1.233	954.6
−80.	1252.3	91.513	91.593	.534 67	0.8238	1.250	907.0
−70.	1226.8	104.11	104.19	.598 27	0.8345	1.270	859.4
−60.	1200.7	116.92	117.01	.659 83	0.8470	1.293	811.8
−50.	1173.9	129.97	130.05	.719 65	0.8608	1.318	764.0
−47.518	1167.1	133.25	133.33	.734 26	0.8644	1.324	752.1
−47.518	4.7099	338.92	360.15	1.7395	0.7123	0.8433	154.5
−40.	4.5290	344.44	366.52	1.7673	0.7239	0.8500	157.5
−30.	4.3130	351.89	375.07	1.8032	0.7399	0.8610	161.2
−20.	4.1200	359.47	383.74	1.8381	0.7565	0.8738	164.8
−10.	3.9460	367.21	392.55	1.8723	0.7738	0.8880	168.2
0.	3.7880	375.11	401.51	1.9057	0.7918	0.9036	171.5
10.	3.6435	383.18	410.63	1.9385	0.8102	0.9201	174.7
20.	3.5106	391.43	419.91	1.9707	0.8290	0.9374	177.8
30.	3.3878	399.86	429.38	2.0024	0.8479	0.9551	180.9
40.	3.2739	408.47	439.02	2.0337	0.8669	0.9731	183.8
50.	3.1678	417.27	448.84	2.0646	0.8859	0.9912	186.7
60.	3.0687	426.25	458.84	2.0951	0.9047	1.009	189.6
70.	2.9759	435.42	469.02	2.1252	0.9234	1.027	192.4
80.	2.8888	444.77	479.39	2.1550	0.9418	1.045	195.1
90.	2.8068	454.30	489.93	2.1844	0.9600	1.063	197.8
100.	2.7295	464.01	500.65	2.2135	0.9780	1.081	200.4
150.	2.4002	515.16	556.82	2.3547	1.063	1.165	213.1
200.	2.1430	570.34	617.01	2.4890	1.141	1.241	225.0
250.	1.9360	629.18	680.83	2.6172	1.210	1.310	236.3
300.	1.7659	691.29	747.92	2.7396	1.272	1.372	247.0
			0.2 MPa				
−100.	1302.2	66.816	66.970	.399 70	0.8117	1.220	1002.5
−90.	1277.6	79.073	79.229	.468 53	0.8159	1.233	955.0
−80.	1252.5	91.482	91.642	.534 51	0.8239	1.250	907.5
−70.	1227.0	104.08	104.24	.598 10	0.8345	1.270	860.0
−60.	1200.9	116.88	117.05	.659 65	0.8470	1.292	812.4
−50.	1174.2	129.93	130.10	.719 46	0.8609	1.317	764.6
−40.	1146.6	143.23	143.40	.777 78	0.8756	1.345	716.7
−31.774	1123.1	154.39	154.56	.824 83	0.8883	1.370	677.1
−31.774	9.0691	347.87	369.92	1.7170	0.7633	0.9145	155.8
−30.	8.9809	349.27	371.54	1.7237	0.7650	0.9139	156.6
−20.	8.5237	357.22	380.68	1.7606	0.7767	0.9157	160.7
−10.	8.1226	365.25	389.87	1.7962	0.7905	0.9224	164.7
0.	7.7659	373.39	399.14	1.8307	0.8055	0.9319	168.4
10.	7.4452	381.65	408.52	1.8644	0.8214	0.9436	171.9
20.	7.1543	390.06	418.02	1.8974	0.8381	0.9570	175.3
30.	6.8886	398.63	427.66	1.9298	0.8554	0.9716	178.6
40.	6.6443	407.35	437.45	1.9615	0.8731	0.9871	181.8
50.	6.4188	416.24	447.40	1.9928	0.8910	1.003	184.9
60.	6.2094	425.31	457.52	2.0236	0.9090	1.020	187.9
70.	6.0145	434.54	467.80	2.0540	0.9270	1.036	190.8
80.	5.8324	443.96	478.25	2.0841	0.9449	1.053	193.7
90.	5.6617	453.54	488.86	2.1137	0.9627	1.070	196.5
100.	5.5013	463.30	499.65	2.1430	0.9803	1.087	199.2
150.	4.8238	514.61	556.07	2.2848	1.064	1.169	212.3
200.	4.2994	569.90	616.41	2.4195	1.141	1.244	224.5
250.	3.8800	628.81	680.35	2.5479	1.210	1.312	235.9
300.	3.5363	690.97	747.53	2.6705	1.273	1.374	246.8
			0.5 MPa				
−100.	1302.6	66.741	67.125	.399 26	0.8119	1.219	1003.6
−90.	1278.1	78.989	79.380	.468 07	0.8161	1.233	956.4
−80.	1253.1	91.389	91.788	.534 03	0.8240	1.250	909.0

Thermodynamic Properties of R-143a—Continued

t (°C)	ρ (kg/m^3)	u (kJ/kg)	h (kJ/kg)	s (kJ/(kg K))	c_v (kJ/(kg K))	c_p (kJ/(kg K))	w (m/s)
−70.	1227.6	103.97	104.38	.597 59	0.8347	1.269	861.7
−60.	1201.6	116.77	117.18	.659 10	0.8472	1.292	814.2
−50.	1175.0	129.79	130.22	.718 87	0.8610	1.316	766.7
−40.	1147.5	143.08	143.51	.777 15	0.8757	1.343	719.0
−30.	1118.9	156.65	157.10	.834 18	0.8912	1.374	671.0
−20.	1089.0	170.54	171.00	.890 21	0.9072	1.408	622.6
−10.	1057.4	184.80	185.28	.945 52	0.9237	1.448	573.3
−6.714	1046.6	189.58	190.06	.963 58	0.9292	1.463	556.9
−6.714	22.034	361.62	384.32	1.6927	0.8509	1.060	154.3
0.	21.148	367.72	391.36	1.7188	0.8504	1.041	157.9
10.	20.009	376.71	401.70	1.7560	0.8565	1.029	162.8
20.	19.032	385.69	411.96	1.7916	0.8665	1.026	167.2
30.	18.175	394.72	422.23	1.8260	0.8786	1.028	171.4
40.	17.413	403.82	432.54	1.8595	0.8922	1.034	175.3
50.	16.728	413.03	442.92	1.8921	0.9068	1.043	179.0
60.	16.107	422.37	453.41	1.9241	0.9222	1.054	182.6
70.	15.539	431.83	464.01	1.9554	0.9381	1.066	186.0
80.	15.017	441.44	474.73	1.9862	0.9543	1.079	189.3
90.	14.534	451.19	485.59	2.0166	0.9707	1.093	192.5
100.	14.086	461.10	496.59	2.0464	0.9872	1.107	195.6
150.	12.239	512.94	553.79	2.1902	1.068	1.181	209.9
200.	10.851	568.55	614.63	2.3260	1.144	1.252	222.9
250.	9.7595	627.69	678.92	2.4551	1.212	1.318	234.9
300.	8.8753	690.02	746.36	2.5782	1.274	1.378	246.1
				1.0 MPa			
−100.	1303.4	66.617	67.385	.398 55	0.8123	1.219	1005.6
−90.	1278.9	78.851	79.633	.467 31	0.8164	1.232	958.6
−80.	1254.0	91.235	92.032	.533 23	0.8243	1.249	911.5
−70.	1228.7	103.80	104.61	.596 74	0.8349	1.268	864.4
−60.	1202.8	116.57	117.41	.658 19	0.8474	1.290	817.3
−50.	1176.3	129.58	130.43	.717 89	0.8612	1.314	770.1
−40.	1148.9	142.83	143.70	.776 09	0.8759	1.341	722.8
−30.	1120.6	156.37	157.26	.833 02	0.8912	1.371	675.2
−20.	1091.0	170.22	171.13	.888 93	0.9072	1.404	627.3
−10.	1059.8	184.42	185.37	.944 07	0.9236	1.443	578.7
0.	1026.5	199.05	200.03	.998 74	0.9406	1.490	529.0
10.	990.23	214.20	215.21	1.0533	0.9584	1.548	477.5
16.332	965.24	224.12	225.15	1.0880	0.9703	1.595	443.5
16.332	44.787	372.99	395.32	1.6759	0.9384	1.259	148.2
20.	43.508	376.88	399.87	1.6915	0.9316	1.225	150.9
30.	40.582	387.17	411.81	1.7316	0.9256	1.170	157.5
40.	38.219	397.20	423.37	1.7691	0.9286	1.143	163.2
50.	36.234	407.13	434.73	1.8048	0.9361	1.130	168.4
60.	34.524	417.03	446.00	1.8391	0.9461	1.126	173.1
70.	33.023	426.97	457.25	1.8724	0.9579	1.126	177.5
80.	31.688	436.97	468.53	1.9048	0.9709	1.130	181.6
90.	30.487	447.06	479.86	1.9365	0.9847	1.137	185.5
100.	29.396	457.26	491.27	1.9674	0.9991	1.145	189.3
150.	25.111	510.08	549.91	2.1148	1.074	1.203	205.9
200.	22.052	566.28	611.63	2.2526	1.147	1.266	220.2
250.	19.719	625.81	676.52	2.3830	1.215	1.328	233.1
300.	17.865	688.43	744.40	2.5068	1.276	1.386	245.0
				1.5 MPa			
−100.	1304.1	66.494	67.644	.397 83	0.8126	1.218	1007.5
−90.	1279.7	78.714	79.886	.466 56	0.8167	1.231	960.7
−80.	1254.9	91.082	92.277	.532 43	0.8246	1.248	914.0
−70.	1229.7	103.63	104.85	.595 89	0.8351	1.267	867.2
−60.	1203.9	116.38	117.63	.657 29	0.8476	1.289	820.3
−50.	1177.5	129.36	130.64	.716 92	0.8613	1.313	773.4
−40.	1150.4	142.59	143.89	.775 04	0.8760	1.339	726.5
−30.	1122.3	156.09	157.43	.831 88	0.8913	1.368	679.4

Thermodynamic Properties of R-143a—Continued

t (°C)	ρ (kg/m^3)	u (kJ/kg)	h (kJ/kg)	s (kJ/(kg K))	c_v (kJ/(kg K))	c_p (kJ/(kg K))	w (m/s)
−20.	1093.0	169.90	171.27	.887 67	0.9072	1.401	632.0
−10.	1062.1	184.05	185.47	.942 65	0.9235	1.439	584.0
0.	1029.3	198.61	200.07	.997 11	0.9404	1.483	535.1
10.	993.71	213.66	215.17	1.0514	0.9579	1.539	484.7
20.	954.36	229.33	230.90	1.1060	0.9765	1.612	431.9
30.	909.26	245.86	247.51	1.1617	0.9975	1.718	375.0
31.794	900.29	248.95	250.61	1.1719	1.002	1.743	364.1
31.794	70.144	379.17	400.56	1.6636	1.003	1.482	140.9
40.	64.848	388.97	412.10	1.7010	0.9808	1.348	148.5
50.	60.029	400.16	425.15	1.7420	0.9729	1.270	156.0
60.	56.250	410.95	437.62	1.7800	0.9742	1.229	162.5
70.	53.140	421.56	449.79	1.8160	0.9802	1.207	168.2
80.	50.500	432.09	461.79	1.8505	0.9890	1.196	173.4
90.	48.210	442.61	473.72	1.8838	0.9997	1.191	178.2
100.	46.190	453.16	485.63	1.9161	1.012	1.191	182.7
150.	38.678	507.14	545.92	2.0677	1.080	1.227	201.8
200.	33.620	563.98	608.59	2.2076	1.151	1.282	217.6
250.	29.883	623.91	674.11	2.3392	1.217	1.339	231.5
300.	26.969	686.82	742.44	2.4639	1.277	1.394	244.0
			2.0 MPa				
−100.	1304.8	66.372	67.905	.397 12	0.8130	1.217	1009.4
−90.	1280.5	78.577	80.139	.465 81	0.8170	1.230	962.9
−80.	1255.8	90.930	92.523	.531 64	0.8248	1.247	916.4
−70.	1230.7	103.46	105.09	.595 05	0.8354	1.266	869.9
−60.	1205.0	116.19	117.85	.656 40	0.8478	1.288	823.3
−50.	1178.8	129.15	130.85	.715 96	0.8615	1.311	776.8
−40.	1151.8	142.35	144.09	.774 00	0.8761	1.337	730.2
−30.	1123.9	155.82	157.60	.830 74	0.8914	1.366	683.5
−20.	1094.9	169.59	171.41	.886 42	0.9072	1.398	636.5
−10.	1064.4	183.69	185.57	.941 25	0.9235	1.434	589.1
0.	1032.0	198.18	200.12	.995 52	0.9402	1.477	541.0
10.	997.07	213.14	215.14	1.0495	0.9575	1.530	491.6
20.	958.69	228.68	230.76	1.1037	0.9757	1.597	440.2
30.	915.18	245.00	247.18	1.1588	0.9958	1.693	385.5
40.	863.21	262.50	264.82	1.2160	1.020	1.849	324.6
43.748	840.11	269.54	271.92	1.2386	1.031	1.943	298.9
43.748	99.448	382.44	402.55	1.6508	1.059	1.790	133.0
50.	91.768	391.16	412.95	1.6833	1.030	1.565	140.6
60.	83.250	403.66	427.68	1.7282	1.011	1.404	150.1
70.	77.067	415.35	441.30	1.7685	1.007	1.327	157.9
80.	72.207	426.65	454.34	1.8060	1.010	1.285	164.5
90.	68.209	437.74	467.06	1.8415	1.016	1.261	170.4
100.	64.818	448.75	479.60	1.8755	1.025	1.248	175.8
150.	53.013	504.09	541.82	2.0320	1.087	1.253	197.8
200.	45.572	561.63	605.51	2.1742	1.155	1.298	215.1
250.	40.253	622.00	671.69	2.3071	1.219	1.350	229.9
300.	36.186	685.22	740.49	2.4327	1.279	1.402	243.1
			2.5 MPa				
−100.	1305.6	66.250	68.165	.396 41	0.8134	1.217	1011.3
−90.	1281.3	78.442	80.393	.465 07	0.8173	1.230	965.1
−80.	1256.7	90.779	92.769	.530 85	0.8251	1.246	918.9
−70.	1231.7	103.29	105.32	.594 22	0.8356	1.265	872.6
−60.	1206.2	116.01	118.08	.655 51	0.8480	1.286	826.3
−50.	1180.1	128.94	131.06	.715 01	0.8617	1.310	780.1
−40.	1153.3	142.11	144.28	.772 97	0.8763	1.335	733.8
−30.	1125.6	155.55	157.77	.829 63	0.8915	1.363	687.5
−20.	1096.8	169.28	171.56	.885 19	0.9073	1.395	641.0
−10.	1066.6	183.33	185.68	.939 88	0.9235	1.430	594.2
0.	1034.6	197.76	200.18	.993 96	0.9400	1.471	546.7
10.	1000.3	212.63	215.13	1.0477	0.9571	1.521	498.2
20.	962.82	228.05	230.65	1.1016	0.9750	1.585	448.1

Thermodynamic Properties of R-143a—Continued

t (°C)	ρ (kg/m^3)	u (kJ/kg)	h (kJ/kg)	s (kJ/(kg K))	c_v (kJ/(kg K))	c_p (kJ/(kg K))	w (m/s)
30.	920.72	244.19	246.90	1.1561	0.9943	1.671	395.4
40.	871.38	261.35	264.22	1.2123	1.017	1.805	337.9
50.	808.38	280.31	283.40	1.2725	1.048	2.070	270.5
53.596	778.96	287.95	291.16	1.2964	1.064	2.265	240.9
53.596	134.92	383.29	401.82	1.6351	1.115	2.311	124.6
60.	120.59	393.97	414.70	1.6742	1.069	1.807	134.7
70.	107.14	407.85	431.18	1.7229	1.042	1.535	146.0
80.	98.087	420.40	445.88	1.7652	1.034	1.418	154.8
90.	91.249	432.33	459.73	1.8038	1.035	1.356	162.2
100.	85.765	443.95	473.10	1.8401	1.040	1.321	168.7
150.	68.194	500.94	537.60	2.0024	1.093	1.282	193.7
200.	57.922	559.24	602.40	2.1471	1.158	1.314	212.6
250.	50.829	620.08	669.26	2.2814	1.222	1.361	228.4
300.	45.513	683.61	738.54	2.4078	1.281	1.410	242.2
			3.0 MPa				
−100.	1306.3	66.129	68.426	.395 71	0.8137	1.216	1013.2
−90.	1282.1	78.307	80.647	.464 32	0.8176	1.229	967.3
−80.	1257.6	90.629	93.015	.530 07	0.8253	1.245	921.3
−70.	1232.7	103.13	105.56	.593 39	0.8358	1.264	875.3
−60.	1207.3	115.82	118.30	.654 62	0.8482	1.285	829.3
−50.	1181.3	128.73	131.27	.714 06	0.8618	1.308	783.3
−40.	1154.7	141.88	144.48	.771 96	0.8764	1.333	737.4
−30.	1127.2	155.28	157.95	.828 52	0.8916	1.361	691.5
−20.	1098.6	168.98	171.71	.883 97	0.9074	1.392	645.4
−10.	1068.8	182.98	185.79	.938 53	0.9235	1.426	599.1
0.	1037.2	197.35	200.24	.992 43	0.9399	1.466	552.3
10.	1003.5	212.14	215.13	1.0460	0.9568	1.513	504.7
20.	966.78	227.45	230.55	1.0995	0.9744	1.573	455.7
30.	925.94	243.41	246.65	1.1535	0.9931	1.652	404.6
40.	878.81	260.30	263.71	1.2088	1.014	1.768	349.9
50.	820.76	278.65	282.30	1.2672	1.041	1.974	288.3
60.	736.18	300.25	304.32	1.3343	1.089	2.582	208.1
61.996	710.37	305.59	309.81	1.3507	1.108	2.959	185.7
61.996	181.48	381.33	397.86	1.6135	1.176	3.489	115.6
70.	149.44	397.82	417.89	1.6726	1.095	2.018	131.5
80.	130.60	412.89	435.86	1.7242	1.065	1.644	143.9
90.	118.57	426.17	451.47	1.7678	1.056	1.495	153.4
100.	109.74	438.65	465.99	1.8073	1.056	1.417	161.3
150.	84.306	497.67	533.25	1.9765	1.099	1.315	189.8
200.	70.685	556.81	599.26	2.1240	1.162	1.332	210.2
250.	61.612	618.14	666.83	2.2597	1.224	1.373	226.9
300.	54.948	681.99	736.59	2.3870	1.283	1.418	241.4
			3.5 MPa				
−100.	1307.0	66.009	68.687	.395 00	0.8140	1.216	1015.1
−90.	1282.9	78.174	80.902	.463 58	0.8179	1.228	969.4
−80.	1258.5	90.481	93.262	.529 29	0.8256	1.244	923.7
−70.	1233.6	102.96	105.80	.592 56	0.8360	1.263	877.9
−60.	1208.4	115.63	118.53	.653 75	0.8484	1.284	832.2
−50.	1182.5	128.52	131.48	.713 13	0.8620	1.307	786.6
−40.	1156.1	141.65	144.67	.770 95	0.8766	1.332	741.0
−30.	1128.8	155.02	158.12	.827 42	0.8918	1.359	695.4
−20.	1100.5	168.68	171.86	.882 77	0.9074	1.389	649.8
−10.	1070.9	182.64	185.91	.937 20	0.9235	1.422	604.0
0.	1039.7	196.95	200.32	.990 94	0.9398	1.461	557.8
10.	1006.5	211.67	215.14	1.0442	0.9566	1.506	511.0
20.	970.60	226.87	230.47	1.0974	0.9739	1.562	463.1
30.	930.89	242.68	246.44	1.1510	0.9921	1.635	413.4
40.	885.66	259.32	263.27	1.2056	1.012	1.738	361.0
50.	831.41	277.19	281.40	1.2626	1.036	1.905	303.6
60.	758.87	297.38	301.99	1.3253	1.072	2.278	235.3
69.289	615.49	324.82	330.50	1.4096	1.185	6.345	128.8

Thermodynamic Properties of R-143a—Continued

t (°C)	ρ (kg/m^3)	u (kJ/kg)	h (kJ/kg)	s (kJ/(kg K))	c_v (kJ/(kg K))	c_p (kJ/(kg K))	w (m/s)
69.289	257.31	373.85	387.46	1.5759	1.260	9.247	105.5
70.	240.53	378.09	392.64	1.5910	1.228	6.000	109.1
80.	175.65	403.07	423.00	1.6784	1.110	2.130	131.4
90.	152.41	418.89	441.86	1.7311	1.082	1.717	144.0
100.	137.81	432.71	458.10	1.7752	1.074	1.552	153.6
150.	101.44	494.27	528.78	1.9532	1.105	1.352	186.0
200.	83.870	554.35	596.08	2.1035	1.165	1.351	208.0
250.	72.601	616.19	664.39	2.2408	1.226	1.384	225.6
300.	64.488	680.38	734.65	2.3690	1.284	1.426	240.6
			4.0 MPa				
−100.	1307.8	65.889	68.948	.394 30	0.8144	1.215	1017.0
−90.	1283.7	78.041	81.157	.462 85	0.8182	1.227	971.6
−80.	1259.4	90.333	93.509	.528 51	0.8258	1.244	926.1
−70.	1234.6	102.80	106.04	.591 74	0.8363	1.262	880.6
−60.	1209.5	115.45	118.76	.652 88	0.8486	1.283	835.1
−50.	1183.8	128.32	131.70	.712 20	0.8622	1.305	789.8
−40.	1157.4	141.42	144.87	.769 95	0.8767	1.330	744.5
−30.	1130.3	154.76	158.30	.826 34	0.8919	1.356	699.3
−20.	1102.2	168.38	172.01	.881 59	0.9075	1.386	654.1
−10.	1073.0	182.30	186.03	.935 89	0.9235	1.418	608.7
0.	1042.2	196.56	200.39	.989 46	0.9398	1.456	563.2
10.	1009.5	211.20	215.16	1.0426	0.9564	1.499	517.1
20.	974.27	226.31	230.41	1.0955	0.9735	1.552	470.1
30.	935.59	241.98	246.26	1.1486	0.9913	1.620	421.8
40.	892.01	258.40	262.88	1.2026	1.011	1.712	371.4
50.	840.82	275.89	280.64	1.2584	1.033	1.852	317.3
60.	775.88	295.16	300.32	1.3183	1.062	2.118	256.1
70.	673.79	318.90	324.84	1.3908	1.120	3.062	176.4
80.	256.27	387.12	402.73	1.6142	1.189	4.019	115.9
90.	197.33	409.81	430.08	1.6907	1.116	2.129	133.9
100.	171.70	425.87	449.16	1.7425	1.095	1.751	145.8
150.	119.69	490.75	524.17	1.9316	1.111	1.393	182.3
200.	97.487	551.85	592.88	2.0851	1.168	1.370	205.9
250.	83.791	614.22	661.96	2.2239	1.229	1.396	224.4
300.	74.128	678.76	732.72	2.3530	1.286	1.435	240.0
			5.0 MPa				
−100.	1309.2	65.652	69.471	.392 91	0.8150	1.214	1020.7
−90.	1285.3	77.777	81.667	.461 39	0.8187	1.226	975.8
−80.	1261.1	90.041	94.005	.526 97	0.8263	1.242	930.8
−70.	1236.6	102.47	106.51	.590 11	0.8367	1.260	885.8
−60.	1211.6	115.09	119.22	.651 15	0.8489	1.281	840.9
−50.	1186.2	127.92	132.13	.710 35	0.8625	1.303	796.1
−40.	1160.1	140.97	145.28	.767 97	0.8770	1.326	751.4
−30.	1133.4	154.26	158.67	.824 20	0.8921	1.352	706.9
−20.	1105.8	167.81	172.33	.879 26	0.9077	1.380	662.4
−10.	1077.1	181.64	186.28	.933 32	0.9235	1.411	618.0
0.	1047.0	195.79	200.57	.986 60	0.9397	1.446	573.5
10.	1015.2	210.31	215.23	1.0393	0.9561	1.487	528.8
20.	981.24	225.23	230.33	1.0917	0.9728	1.535	483.5
30.	944.38	240.66	245.96	1.1441	0.9900	1.593	437.5
40.	903.55	256.72	262.25	1.1970	1.008	1.669	390.2
50.	857.05	273.60	279.44	1.2510	1.028	1.775	341.0
60.	801.65	291.70	297.94	1.3074	1.051	1.940	288.5
70.	730.01	311.87	318.72	1.3688	1.082	2.259	230.4
80.	616.67	337.09	345.19	1.4448	1.139	3.292	161.6
90.	380.30	378.96	392.11	1.5757	1.202	4.830	118.7
100.	270.21	407.92	426.42	1.6690	1.145	2.567	131.7
150.	159.92	483.31	514.58	1.8919	1.124	1.489	175.8
200.	126.03	546.74	586.42	2.0524	1.175	1.412	202.2
250.	106.76	610.27	657.10	2.1944	1.233	1.421	222.2
300.	93.689	675.52	728.89	2.3254	1.289	1.452	238.9

Thermodynamic Properties of R-143a—Continued

t (°C)	ρ (kg/m^3)	u (kJ/kg)	h (kJ/kg)	s (kJ/(kg K))	c_v (kJ/(kg K))	c_p (kJ/(kg K))	w (m/s)
			6.0 MPa				
−100.	1310.6	65.418	69.996	.391 53	0.8157	1.213	1024.5
−90.	1286.9	77.517	82.180	.459 94	0.8193	1.225	980.0
−80.	1262.8	89.752	94.503	.525 45	0.8268	1.240	935.5
−70.	1238.5	102.15	107.00	.588 51	0.8371	1.258	891.0
−60.	1213.7	114.74	119.68	.649 44	0.8493	1.278	846.6
−50.	1188.5	127.52	132.57	.708 54	0.8628	1.300	802.3
−40.	1162.8	140.52	145.68	.766 03	0.8773	1.323	758.2
−30.	1136.4	153.76	159.04	.822 11	0.8924	1.348	714.3
−20.	1109.2	167.24	172.65	.876 98	0.9079	1.375	670.6
−10.	1081.0	181.00	186.55	.930 83	0.9237	1.405	627.0
0.	1051.6	195.06	200.77	.983 83	0.9397	1.438	583.5
10.	1020.6	209.45	215.33	1.0362	0.9559	1.476	539.9
20.	987.79	224.22	230.30	1.0881	0.9724	1.519	496.2
30.	952.46	239.44	245.74	1.1399	0.9891	1.571	452.0
40.	913.87	255.20	261.76	1.1919	1.006	1.636	407.2
50.	870.84	271.63	278.52	1.2446	1.025	1.720	361.4
60.	821.46	288.97	296.27	1.2987	1.044	1.838	314.2
70.	762.27	307.62	315.49	1.3555	1.068	2.021	264.9
80.	686.10	328.43	337.17	1.4178	1.098	2.354	213.0
90.	576.35	353.44	363.85	1.4922	1.140	3.069	161.5
100.	429.17	383.98	397.96	1.5849	1.168	3.449	134.8
150.	205.54	475.36	504.55	1.8551	1.135	1.604	170.9
200.	156.28	541.52	579.92	2.0236	1.181	1.457	199.3
250.	130.45	606.29	652.29	2.1690	1.237	1.447	220.6
300.	113.58	672.29	725.12	2.3020	1.292	1.469	238.1
			8.0 MPa				
−100.	1313.4	64.957	71.048	.388 80	0.8169	1.210	1031.9
−90.	1289.9	77.006	83.208	.457 08	0.8203	1.222	988.4
−80.	1266.2	89.186	95.504	.522 44	0.8277	1.237	944.8
−70.	1242.2	101.52	107.97	.585 34	0.8379	1.255	901.2
−60.	1217.9	114.04	120.61	.646 10	0.8500	1.274	857.7
−50.	1193.1	126.75	133.46	.704 99	0.8635	1.295	814.4
−40.	1167.9	139.67	146.52	.762 24	0.8779	1.317	771.4
−30.	1142.2	152.80	159.80	.818 04	0.8929	1.341	728.7
−20.	1115.7	166.17	173.34	.872 58	0.9083	1.366	686.3
−10.	1088.5	179.79	187.13	.926 03	0.9240	1.394	644.2
0.	1060.2	193.67	201.22	.978 55	0.9398	1.423	602.4
10.	1030.8	207.85	215.61	1.0303	0.9558	1.456	560.9
20.	999.80	222.36	230.36	1.0815	0.9719	1.494	519.5
30.	966.98	237.23	245.50	1.1323	0.9881	1.536	478.3
40.	931.83	252.52	261.11	1.1829	1.004	1.586	437.1
50.	893.74	268.30	277.25	1.2337	1.021	1.646	396.1
60.	851.86	284.67	294.06	1.2849	1.038	1.719	355.1
70.	805.00	301.77	311.71	1.3371	1.056	1.813	314.4
80.	751.53	319.78	330.43	1.3908	1.075	1.937	274.2
90.	689.32	338.97	350.57	1.4471	1.095	2.100	235.7
100.	616.43	359.58	372.56	1.5068	1.117	2.300	201.4
150.	311.31	458.51	484.21	1.7884	1.152	1.847	169.5
200.	221.20	530.92	567.08	1.9738	1.191	1.550	196.8
250.	179.62	598.35	642.89	2.1262	1.244	1.498	219.3
300.	154.14	665.90	717.80	2.2629	1.298	1.503	237.9
			10 MPa				
−100.	1316.2	64.506	72.103	.386 12	0.8181	1.208	1039.2
−90.	1293.0	76.507	84.241	.454 26	0.8213	1.220	996.6
−80.	1269.5	88.635	96.512	.519 49	0.8286	1.235	953.9
−70.	1245.8	100.92	108.94	.582 24	0.8387	1.252	911.2
−60.	1221.9	113.37	121.55	.642 83	0.8507	1.270	868.5
−50.	1197.6	126.01	134.36	.701 53	0.8641	1.291	826.2
−40.	1172.9	138.84	147.37	.758 56	0.8785	1.312	784.1

Thermodynamic Properties of R-143a—Continued

t (°C)	ρ (kg/m^3)	u (kJ/kg)	h (kJ/kg)	s (kJ/(kg K))	c_v (kJ/(kg K))	c_p (kJ/(kg K))	w (m/s)
−30.	1147.7	151.88	160.60	.814 11	0.8934	1.334	742.5
−20.	1122.0	165.14	174.06	.868 36	0.9087	1.358	701.3
−10.	1095.5	178.64	187.76	.921 46	0.9243	1.384	660.5
0.	1068.3	192.37	201.73	.973 56	0.9401	1.411	620.1
10.	1040.1	206.37	215.99	1.0248	0.9559	1.441	580.3
20.	1010.7	220.66	230.56	1.0754	0.9718	1.473	540.8
30.	979.81	235.26	245.46	1.1254	0.9877	1.509	501.8
40.	947.23	250.20	260.75	1.1750	1.004	1.550	463.3
50.	912.56	265.52	276.48	1.2244	1.019	1.596	425.4
60.	875.35	281.28	292.70	1.2738	1.035	1.649	388.1
70.	835.08	297.52	309.50	1.3235	1.051	1.711	351.8
80.	791.16	314.32	326.96	1.3737	1.068	1.783	316.7
90.	742.98	331.74	345.20	1.4246	1.084	1.866	283.6
100.	690.23	349.82	364.31	1.4765	1.100	1.956	253.3
150.	419.13	442.95	466.81	1.7343	1.158	1.952	184.2
200.	289.41	520.48	555.04	1.9317	1.199	1.633	199.6
250.	230.20	590.56	634.00	2.0904	1.250	1.546	220.7
300.	195.24	659.65	710.87	2.2307	1.303	1.535	239.3
			15 MPa				
−100.	1322.9	63.419	74.758	.379 56	0.8207	1.204	1057.1
−90.	1300.3	75.308	86.844	.447 42	0.8235	1.214	1016.6
−80.	1277.5	87.315	99.057	.512 34	0.8305	1.228	975.9
−70.	1254.6	99.464	111.42	.574 75	0.8404	1.245	935.2
−60.	1231.4	111.77	123.95	.634 96	0.8523	1.262	894.5
−50.	1208.1	124.25	136.67	.693 25	0.8656	1.281	854.2
−40.	1184.5	136.91	149.57	.749 81	0.8799	1.300	814.3
−30.	1160.6	149.75	162.67	.804 83	0.8947	1.320	774.9
−20.	1136.3	162.78	175.98	.858 46	0.9100	1.341	736.1
−10.	1111.6	176.01	189.50	.910 86	0.9255	1.363	697.9
0.	1086.4	189.44	203.25	.962 13	0.9411	1.386	660.5
10.	1060.6	203.09	217.23	1.0124	0.9568	1.410	623.8
20.	1034.1	216.96	231.47	1.0618	0.9724	1.436	587.8
30.	1006.8	231.06	245.96	1.1104	0.9880	1.463	552.7
40.	978.61	245.40	260.72	1.1583	1.003	1.491	518.5
50.	949.36	259.98	275.79	1.2057	1.019	1.521	485.3
60.	918.94	274.83	291.16	1.2525	1.034	1.553	453.2
70.	887.26	289.95	306.85	1.2989	1.049	1.587	422.4
80.	854.21	305.34	322.90	1.3450	1.063	1.622	393.2
90.	819.77	321.00	339.30	1.3908	1.078	1.658	365.7
100.	783.98	336.92	356.05	1.4363	1.092	1.693	340.2
150.	596.24	418.88	444.04	1.6575	1.156	1.795	252.9
200.	445.13	498.46	532.16	1.8544	1.209	1.712	230.2
250.	352.90	572.91	615.41	2.0217	1.262	1.628	237.0
300.	295.92	645.18	695.87	2.1686	1.313	1.597	250.6
			20 MPa				
−100.	1329.3	62.387	77.432	.373 23	0.8229	1.199	1074.5
−90.	1307.3	74.173	89.473	.440 83	0.8254	1.210	1036.0
−80.	1285.1	86.070	101.63	.505 48	0.8322	1.223	997.1
−70.	1262.8	98.101	113.94	.567 59	0.8420	1.238	958.1
−60.	1240.4	110.28	126.41	.627 49	0.8538	1.255	919.1
−50.	1217.9	122.62	139.04	.685 43	0.8670	1.273	880.5
−40.	1195.2	135.12	151.86	.741 60	0.8812	1.291	842.4
−30.	1172.4	147.80	164.86	.796 20	0.8960	1.309	804.9
−20.	1149.3	160.64	178.05	.849 35	0.9112	1.329	768.0
−10.	1126.0	173.67	191.43	.901 20	0.9267	1.348	731.9
0.	1102.3	186.87	205.01	.951 85	0.9423	1.368	696.6
10.	1078.3	200.25	218.80	1.0014	0.9580	1.389	662.1
20.	1053.9	213.82	232.80	1.0500	0.9736	1.411	628.6
30.	1029.0	227.58	247.01	1.0977	0.9891	1.433	596.0
40.	1003.6	241.52	261.45	1.1445	1.004	1.455	564.5
50.	977.65	255.66	276.12	1.1906	1.020	1.478	534.1

Thermodynamic Properties of R-143a—Continued

t (°C)	ρ (kg/m^3)	u (kJ/kg)	h (kJ/kg)	s (kJ/(kg K))	c_v (kJ/(kg K))	c_p (kJ/(kg K))	w (m/s)
60.	951.09	269.99	291.02	1.2360	1.035	1.502	504.9
70.	923.89	284.51	306.16	1.2808	1.049	1.526	477.0
80.	896.04	299.21	321.54	1.3250	1.064	1.550	450.5
90.	867.57	314.10	337.15	1.3686	1.078	1.574	425.6
100.	838.53	329.16	353.01	1.4117	1.092	1.597	402.4
150.	689.70	406.22	435.22	1.6183	1.157	1.680	315.3
200.	555.91	483.56	519.54	1.8067	1.215	1.682	275.7
250.	456.09	558.95	602.81	1.9740	1.269	1.649	266.8
300.	386.50	632.94	684.68	2.1235	1.321	1.629	271.5
				25 MPa			
−90.	1313.9	73.095	92.122	.434 47	0.8270	1.205	1054.8
−80.	1292.3	84.892	104.24	.498 87	0.8336	1.218	1017.5
−70.	1270.6	96.817	116.49	.560 73	0.8433	1.233	980.0
−60.	1248.9	108.88	128.90	.620 36	0.8550	1.249	942.6
−50.	1227.1	121.10	141.47	.678 00	0.8682	1.266	905.5
−40.	1205.2	133.47	154.22	.733 85	0.8824	1.283	868.9
−30.	1183.2	146.00	167.13	.788 09	0.8972	1.300	832.9
−20.	1161.1	158.69	180.23	.840 86	0.9124	1.318	797.6
−10.	1138.9	171.55	193.50	.892 28	0.9279	1.336	763.1
0.	1116.5	184.56	206.95	.942 46	0.9436	1.355	729.5
10.	1093.9	197.74	220.59	.991 49	0.9592	1.373	696.8
20.	1071.1	211.08	234.42	1.0395	0.9749	1.392	665.1
30.	1048.0	224.58	248.43	1.0865	0.9904	1.411	634.4
40.	1024.6	238.24	262.64	1.1326	1.006	1.431	604.8
50.	1000.9	252.07	277.05	1.1779	1.021	1.450	576.3
60.	976.91	266.05	291.64	1.2224	1.036	1.469	549.0
70.	952.58	280.19	306.43	1.2661	1.051	1.489	522.9
80.	927.93	294.48	321.42	1.3092	1.066	1.508	498.2
90.	902.99	308.91	336.59	1.3515	1.080	1.527	474.9
100.	877.79	323.47	351.95	1.3932	1.094	1.545	453.0
150.	750.75	397.85	431.15	1.5923	1.160	1.616	367.6
200.	632.98	473.31	512.80	1.7747	1.220	1.643	320.7
250.	536.58	548.39	594.98	1.9398	1.276	1.642	301.7
300.	462.96	622.99	676.99	2.0895	1.327	1.639	298.1
				50 MPa			
−80.	1324.2	79.790	117.55	.468 89	0.8378	1.201	1111.3
−70.	1304.7	91.302	129.63	.529 85	0.8473	1.214	1079.7
−60.	1285.3	102.94	141.84	.588 54	0.8590	1.229	1047.8
−50.	1266.1	114.71	154.20	.645 21	0.8723	1.243	1016.0
−40.	1246.9	126.61	166.71	.700 04	0.8866	1.258	984.6
−30.	1228.0	138.65	179.37	.753 20	0.9017	1.273	953.8
−20.	1209.1	150.82	192.17	.804 80	0.9172	1.288	923.7
−10.	1190.4	163.12	205.12	.854 98	0.9330	1.303	894.3
0.	1171.9	175.55	218.22	.903 83	0.9489	1.317	865.9
10.	1153.4	188.11	231.46	.951 44	0.9650	1.331	838.3
20.	1135.1	200.80	244.85	.997 89	0.9810	1.346	811.8
30.	1116.9	213.61	258.37	1.0433	0.9969	1.360	786.2
40.	1098.8	226.53	272.04	1.0876	1.013	1.373	761.6
50.	1080.8	239.58	285.84	1.1310	1.028	1.387	738.0
60.	1063.0	252.74	299.77	1.1735	1.044	1.400	715.4
70.	1045.2	266.01	313.84	1.2151	1.059	1.413	693.8
80.	1027.6	279.38	328.04	1.2558	1.074	1.426	673.2
90.	1010.1	292.87	342.36	1.2958	1.089	1.439	653.6
100.	992.79	306.45	356.81	1.3351	1.104	1.451	635.1
150.	908.50	375.75	430.78	1.5210	1.174	1.506	556.8
200.	829.62	447.01	507.28	1.6919	1.238	1.552	501.0
250.	757.93	519.83	585.80	1.8496	1.295	1.588	463.6
300.	694.43	593.97	665.97	1.9959	1.348	1.618	440.1
				75 MPa			
−60.	1315.1	98.202	155.23	.561 19	0.8606	1.218	1139.2
−50.	1297.4	109.67	167.48	.617 35	0.8742	1.232	1110.8

Thermodynamic Properties of R-143a—Continued

t (°C)	ρ (kg/m^3)	u (kJ/kg)	h (kJ/kg)	s (kJ/(kg K))	c_v (kJ/(kg K))	c_p (kJ/(kg K))	w (m/s)
−40.	1279.9	121.28	179.87	.671 66	0.8889	1.246	1082.6
−30.	1262.7	133.01	192.41	.724 30	0.9043	1.260	1054.7
−20.	1245.7	144.87	205.08	.775 37	0.9202	1.274	1027.5
−10.	1229.0	156.86	217.89	.825 00	0.9364	1.288	1001.0
0.	1212.5	168.98	230.84	.873 29	0.9527	1.301	975.3
10.	1196.1	181.22	243.92	.920 32	0.9691	1.315	950.4
20.	1180.1	193.57	257.13	.966 17	0.9854	1.328	926.4
30.	1164.2	206.05	270.47	1.0109	1.002	1.341	903.3
40.	1148.5	218.64	283.94	1.0546	1.018	1.353	881.1
50.	1133.1	231.34	297.53	1.0974	1.034	1.366	859.7
60.	1117.8	244.16	311.25	1.1392	1.050	1.378	839.3
70.	1102.8	257.08	325.09	1.1801	1.066	1.390	819.7
80.	1088.0	270.11	339.04	1.2202	1.081	1.401	801.0
90.	1073.3	283.24	353.12	1.2595	1.096	1.413	783.2
100.	1058.9	296.48	367.30	1.2980	1.111	1.424	766.1
150.	989.77	364.09	439.86	1.4804	1.183	1.477	692.6
200.	925.72	433.91	514.92	1.6480	1.248	1.524	636.4
250.	866.92	505.68	592.19	1.8032	1.307	1.566	594.5
300.	813.40	579.19	671.40	1.9478	1.360	1.602	564.1
			100 MPa				
−50.	1323.8	105.50	181.04	.592 66	0.8748	1.226	1195.5
−40.	1307.5	116.89	193.37	.646 70	0.8900	1.240	1169.3
−30.	1291.5	128.41	205.84	.699 07	0.9059	1.254	1143.5
−20.	1275.7	140.06	218.45	.749 88	0.9222	1.268	1118.1
−10.	1260.2	151.84	231.19	.799 25	0.9387	1.281	1093.4
0.	1245.0	163.75	244.07	.847 28	0.9554	1.294	1069.5
10.	1230.0	175.78	257.08	.894 05	0.9721	1.307	1046.2
20.	1215.3	187.93	270.22	.939 64	0.9888	1.320	1023.8
30.	1200.9	200.21	283.48	.984 13	1.005	1.333	1002.2
40.	1186.7	212.60	296.87	1.0276	1.022	1.345	981.4
50.	1172.7	225.10	310.37	1.0700	1.038	1.357	961.5
60.	1159.0	237.72	324.00	1.1116	1.054	1.369	942.3
70.	1145.5	250.45	337.75	1.1522	1.070	1.380	924.0
80.	1132.2	263.28	351.61	1.1920	1.086	1.392	906.4
90.	1119.2	276.23	365.58	1.2310	1.101	1.403	889.6
100.	1106.3	289.28	379.67	1.2693	1.117	1.414	873.5
150.	1045.3	356.04	451.70	1.4504	1.189	1.466	803.2
200.	989.19	425.14	526.23	1.6168	1.255	1.514	747.8
250.	937.69	496.37	603.02	1.7711	1.314	1.557	704.6
300.	890.50	569.53	681.83	1.9149	1.368	1.595	671.2